Upscale Impact of Mesoscale Disturbances of Tropical Convection on 2-Day Waves

Qiu Yang*

Center for Prototype Climate Modeling, New York University Abu Dhabi, Saadiyat Island, Abu Dhabi, UAE

Andrew J. Majda

Department of Mathematics and Center for Atmosphere Ocean Science, Courant Institute of Mathematical Sciences, New York University, New York, NY, USA,

Center for Prototype Climate Modeling, New York University Abu Dhabi, Saadiyat Island, Abu Dhabi, UAE

**Corresponding author address:* Qiu Yang, Courant Institute of Mathematical Sciences, New York University, 251 Mercer Street, New York, NY, 10012

E-mail: yangq@cims.nyu.edu

ABSTRACT

Westward-propagating 2-day waves with embedded mesoscale disturbances contribute a large portion of synoptic variability of tropical convection over the western Pacific. It is of crucial importance to assess the upscale impact on 2-day waves of these mesoscale disturbances that propagate at various tilt angles. Also, it will be informative to consider the upscale impact on both symmetric and asymmetric 2-day waves in terms of convection, morphology of circulation and tropical cyclogenesis. A simple multi-scale asymptotic model is used to simulate the two-scale structure of 2-day waves. The synoptic-scale circulation response is driven by westward-propagating mean heating and eddy transfer of momentum and temperature. The latter is interpreted as the upscale impact of mesoscale fluctuations. The upscale impact of mesoscale disturbances that propagate at a tilt angle between 315° and 45° induces low-level negative potential temperature anomalies and westerly inflow. Shallow congestus convection triggered in a moist environment at the leading edge of the 2-day waves supports the westward propagation. For asymmetric 2-day waves in the Northern Hemisphere, the upscale impact of mesoscale disturbances propagating at a tilt angle between 315° and 0° induces lower-tropospheric cyclonic flows and negative pressure perturbation. This provides a new mechanism to precondition tropical cyclogenesis. Comparison of the upscale impact on symmetric westward-propagating 2-day waves compared to eastward-propagating convectively coupled Kelvin waves shows that their tilt angle ranges with favorable conditions for convection and enhanced inflow are simply opposite.

1. Introduction

Superclusters of cloudiness over several thousand kilometers frequently observed in the tropics have dramatic impact on local weather and global climate due to large amounts of rainfall (Nakazawa 1988; Mapes and Houze 1993). It is now well understood that these superclusters are organized by the coupling between equatorially trapped waves and tropical convection (Matsuno 1966; Takayabu 1994a; Wheeler et al. 2000; Roundy and Frank 2004; Yang et al. 2007a,b,c; Kiladis et al. 2009), such as eastward-propagating convectively coupled Kelvin waves (CCKWs) (Straub and Kiladis 2002). The 2-day waves are key components of westward-propagating superclusters, which prevail over the western Pacific (WP) (Takayabu 1994b; Takayabu et al. 1996), especially during the active phase of the Madden-Julian Oscillation (MJO) (Schrage et al. 2001; Clayson et al. 2002). Observational studies have been based on satellite infrared data and *in situ* surface measurements from the Tropical Ocean Global Atmosphere Coupled Ocean-Atmosphere Response Experiment (TOGA COARE) (Chen et al. 1996; Takayabu et al. 1996; Chen and Houze 1997; Haertel and Johnson 1998; Clayson et al. 2002). Takayabu (1994b) recognized that 2-day waves have $n = 1$ westward-propagating inertio-gravity (WIG) wave properties. Chen and Houze (1997) called the spatially selective behavior of the large convective systems *diurnal dancing*, and concluded that the 2-day period is determined by the boundary-layer recovery phase. Stechmann and Majda (2009) explained the preferred westward propagation of 2-day waves in terms of the effects of wind shear and gravity waves that create more favorable conditions on one side of convective systems.

Multi-scale organization of tropical convection shed new light on understanding 2-day waves. Chen et al. (1996) observed that the 2-day disturbances extensively contain cloud clusters, the dominant rainfall producer in the tropics (Tao and Moncrieff 2009), most of which moved westward. For cluster-supercluster interactions, Yang and Majda (2018) accessed the upscale impact of embedded mesoscale tropical convection on CCKWs based on a simple multi-scale model. Early studies about scale interactions of atmospheric flows included wave-mean flow interactions (Andrews and McIntyre 1976a,b, 1978a,b,c). Majda (2007) showed that nonlinear interactions across scales that drive the waves include eddy flux divergences of momentum and temperature from the smaller-scale systems as well as large-scale effects. The multi-scale structure of 2-day waves with embedded mesoscale disturbances considered here are illustrated in the conceptual diagram in Fig.1.

Besides the symmetric $n = 1$ WIGs, recent studies based on satellite-observed outgoing long-wave radiation (OLR) show the existence of asymmetric $n = 2$ WIGs with significant spectral signals close to the 2-day period (Wheeler and Kiladis 1999; Wheeler et al. 2000; Kiladis et al. 2009). Kiladis et al. (2009) showed that heavy rainfall identified by the annual mean variance of brightness temperature filtered for the WIG bands occurs widely in equatorial regions, including the WP from $10°S$ to $10°N$. Roundy and Frank (2004) showed that spectral signals of WIGs are more significant in the Northern Hemisphere (NH) than the Southern Hemisphere (SH). This suggests a connection between asymmetric 2-day waves and tropical cyclogenesis in the NH. Frank and Roundy (2006) concluded that tropical cyclone formation is closely related to enhanced wave activity. Dunkerton and his collaborators studied tropical cyclogenesis in a tropical wave crtical layer, particularly easterly waves, focusing on flow kinematics and dynamics, moist thermodynamics and wave/vortex interactions (Dunkerton et al. 2008, 2009; Wang et al. 2010; Lussier III et al. 2015). It is necessary to investigate how 2-day waves with embedded mesoscale disturbances influences tropical cyclogenesis.

Due to their coarse resolution, most GCMs cannot explicitly resolve MCSs and have to rely on cumulus parameterization. Inadequate treatment of MCSs and their upscale impact on the large-scale circulation may explain systematical precipitation bias in GCMs (Dai 2006; Lin 2007; Li and Xie 2014; Woelfle et al. 2018). As an important component of high-frequency variability within the large-scale convective envelope of MJOs (Zhang 2005), 2-day waves that include the effect of mesoscale disturbances may improve the treatment of MJOs. Improved WIG simulations by Khouider and Majda (2008a) is based on the multicloud model parameterization (Khouider and Majda 2006c,a,b, 2008a,b; Khouider et al. 2010, 2011). The Moncrieff et al. (2017) new approach for parameterizing upscale effects of organized tropical convection showed promising improvement in representing large-scale precipitation and tropical wave modes in GCMs.

The goals of this paper include four aspects: First, a simple multi-scale framework models the synoptic-scale 2-day waves with embedded mesoscale disturbances; secondly, the upscale impact of mesoscale disturbances that propagate at various tilt angles on 2-day waves is assessed in terms of favorable conditions for convection, circulation morphology and tropical cyclogenesis; thirdly, the upscale impact of mesoscale disturbances on asymmetric 2-day waves that propagate off the equator in the NH is investigated. Lastly, the upscale impact of mesoscale disturbances on westward-propagating 2-day waves versus eastward-propagating CCKWs is compared.

Early studies of the multi-scale formalism in atmospheric sciences include Quasi-Biennial Oscillations (Plumb and Bell 1982; Lindzen 1987; Takahashi and Holton 1991). The mesoscale equatorial synoptic dynamics (MESD) model derived by Majda (2007) for studying cluster-supercluster interactions is used here. Inspired by the observed self-similarity of clusters, superclusters and intraseasonal oscillations, multi-scale models based on multi-scale asymptotic methods (Majda and Klein 2003; Majda 2007) have studied complex multiple spatiotemporal scale interactions of tropical convection ranging from the mesoscale to the synoptic scales to the intraseasonal/planetary scales (Majda and Biello 2004; Biello and Majda 2005, 2006, 2010; Yang and Majda 2014; Majda and Yang 2016; Yang et al. 2017). The MESD model highlights eddy transfer of momentum and temperature in driving synoptic-scale circulation, which concerns the upscale impact of mesoscale fluctuations. Yang and Majda (2017) used the two-dimensional version of the MESD model to simulate eastward-propagating synoptic-scale superclusters with embedded westward-propagating mesoscale disturbances. They successfully reproduced key features of convective systems with a front-to-rear tilt while compared well with results from a cloud-resolving model (Grabowski and Moncrieff 2001). Yang and Majda (2018) used the three-dimensional version of the MESD to study the upscale impact on CCKWs of mesoscale disturbances propagating at various tilt angles and speeds. In contrast to the eastward-propagating CCKWs in Yang and Majda (2018), herein the MESD model is configured to represent 2-day waves with a westward-propagating convective envelope and embedded mesoscale disturbances propagating at various tilt angles. Both symmetric (along the equator) and asymmetric (off the equator) 2-day waves are examined.

Several crucial results have been obtained pertain to a moist environment by comparing the mean heating driven 2-day waves with the superimposed flow field anomalies induced by eddy transfer of momentum and temperature. First, explicit expressions for eddy transfer of momentum and temperature from mesoscale fluctuations are obtained. Secondly, for symmetric 2-day waves, the upscale impact of mesoscale disturbances propagating at the tilt angle range ($315^\circ \sim 0^\circ$ and $0^\circ \sim 45^\circ$, close to the eastward direction) induces low-level negative potential temperature anomalies around 2-3 *km* to the west, providing favorable conditions to trigger shallow congestus convection in the leading edge and explaining the favored westward propagation other than eastward propagation. Additional westerly inflow induced by this upscale impact around 5 *km* feeds moisture toward the convective envelope to generate convective available potential energy (CAPE). Thirdly, for asymmetric 2-day waves, the upscale impact of mesoscale disturbances propagating at the tilt angle range ($315^\circ \sim 0^\circ$) induces east-southward jets accompanied by cyclonic flows and negative pressure perturbation at equatorial latitudes of the NH, a possible precondition for tropical cyclogenesis. Lastly, comparison between symmetric westward-propagating 2-day waves and eastward-propagating CCKWs shows the anticipated result that their tilt angle ranges with favorable conditions for convection and enhanced inflow are simply opposite in direction.

The results of this paper is presented as follows. Section 2 summarizes properties of the MESD model and explicit expressions of eddy transfer of momentum and temperature (Yang and Majda 2018). Section 3 discusses the synoptic-scale circulation response to the westward-propagating mean heating and upscale impact of embedded mesoscale disturbances propagating at various tilt angles. Section 4 considers asymmetric 2-day waves where the convective envelope propagates westward off the equator in the NH. Section 5 compares the upscale impact of mesoscale disturbances on westward-propagating 2-day waves versus eastward-propagating CCKWs. The paper concludes with discussion in Section 6.

2. Properties of the MESD Model

The MESD model originally derived by Majda (2007) is based on multi-scale asymptotic methods. The derivation starts from the primitive equations, undertakes asymptotic expansions with respect to the small Froude number ($\varepsilon = 0.1$) and defines a multi-scale framework that includes the mesoscale and synoptic scales. The essential physical intuition behind the derivation includes the multi-scale organization of tropical convection and self-similarity properties across scales (Mapes et al. 2006; Majda 2007). The application of its two-dimensional and three-dimensional versions for CCKWs validate the appropriateness of the MESD model to investigate cluster-superclusters interactions (Yang and Majda 2017, 2018). The MESD model consists of two groups of equations: one governs synoptic-scale dynamics and the other mesoscale dynamics. As for the scale analysis, the synoptic space and time scale are $(1500km, 8.3hrs)$, 10 times of those on the mesoscale, $(150km, 50min)$. Horizontal velocity on the synoptic- and meso-scale share the same scaling of

$5ms^{-1}$, while vertical velocity on the mesoscale has scaling of $1.6\times10^{-1}ms^{-1}$, 10 times of that on the synoptic scale ($1.6\times10^{-2}ms^{-1}$). Potential temperature anomalies share the same $3.3K$ scaling, while diabatic heating on the mesoscale has a $100Kday^{-1}$ scaling, 10 times of that on the synoptic scale ($10Kday^{-1}$) (Robert 1982; Yanai and Johnson 1993). For simplicity, the Boussinesq approximation is used as a simple demonstration, although it should account for quasi-compressibility in reality.

The governing equations for synoptic-scale dynamics in dimensionless units are as follows,

$$U_t - YV = -P_X - dU - \left\langle \overline{w'u'} \right\rangle_z, \tag{1a}$$

$$V_t + YU = -P_Y - dV - \left\langle \overline{w'v'} \right\rangle_z, \tag{1b}$$

$$\Theta_t + W = -\left\langle \overline{w'\theta'} \right\rangle_z + S^\theta, \tag{1c}$$

$$P_z = \Theta, \tag{1d}$$

$$U_X + V_Y + W_z = 0, \tag{1e}$$

where $d = \frac{1}{1\,day}$ is a damping coefficient for boundary layer turbulent drag and it is set as a constant for simplicity. S^θ represents synoptic-scale diabatic heating from latent heat release. Such a thermally forced and momentum damped model for synoptic-scale circulation response is consistent with Haertel et al. (2008) in regard to 2-day waves. The notation bar and angle bracket in Eqs.1a-1c denote mesoscale horizontal- and temporal-averaging operators, respectively. For an arbitrary function f,

$$\bar{f}(X,Y) = \lim_{L\to\infty} \frac{1}{4L^2} \int_{-L}^{L} \int_{-L}^{L} f(X,x,Y,y)\,dxdy, \tag{2}$$

$$\langle f \rangle (t) = \lim_{T\to\infty} \frac{1}{2T} \int_{-T}^{T} f(t,\tau)\,d\tau, \tag{3}$$

where L,T denote length of the mesoscale domain and time interval. In the asymptotic limit, all mesoscale fluctuations of f satisfy $\bar{f} = 0$ and $\langle f \rangle = 0$ by definition. According to the scaling analysis as mentioned before, those nonlinear advection terms appearing the original governing equations are order ε on the synoptic scale, and are therefore all ignored in accord with asymptotic assumptions (Majda 2007).

The governing equations for mesoscale dynamics in dimensionless units are,

$$u_\tau = -p_x, \tag{4a}$$

$$v_\tau = -p_y, \tag{4b}$$

$$\theta_\tau + w = s^\theta, \tag{4c}$$

$$p_z = \theta, \tag{4d}$$

$$u_x + v_y + w_z = 0, \tag{4e}$$

where s^θ represents mesoscale diabatic heating from latent heat release. Unlike those in Eqs.1a-1e, neither Coriolis force nor momentum damping terms appear in the mesoscale equations, since their magnitudes are at the order of ε and are accordingly neglected as previously stated.

These two groups of equations not only describe the leading-order behavior of circulation response at each scale by a linear system, but also highlight nonlinear eddy terms associated with cross-scale interactions. The synoptic-scale dynamics in Eqs.1a-1e responds to the Coriolis force on the β-plane, containing all dry equatorially trapped waves of Matsuno (1966) provided the momentum damping terms and eddy terms are ignored. The three eddy terms, $-\left\langle\overline{w'u'}\right\rangle_z, -\left\langle\overline{w'v'}\right\rangle_z, -\left\langle\overline{w'\theta'}\right\rangle_z$ along with the mean heating S^θ drive synoptic-scale dynamics, representing upscale impact of mesoscale fluctuations on synoptic-scale circulation through momentum and heat budget. The mesoscale dynamics in Eqs.4a-4e, that consists only of gravity waves, is thermally driven by the mesoscale heating. The clear scale separation of synoptic- and meso-scale convective systems living on different spatiotemporal scales is the essential feature captured by multi-scale models (Majda and Klein 2003). This multi-scale asymptotic model is valid provided the those diabatic heating does not exceed their corresponding scales. According to the scale analysis with weak advection at order ε, results are insensitive to these heating scales due to the linearity properties of governing equations on both scales. Notably, the original MESD model (Majda 2007) allows a background density vertical profile in the quasi-Boussinesq approximation, which would add an extra factor $e^{-z/2H}$ in front of all variables for a vertically decaying background density $\rho(z) = \rho_0 e^{-z/H}$. In fact, Moncrieff (1985) showed that the effects of vertical variation of density with height can be included implicitly by transforming the quasi-Boussinesq equations from scaled height coordinates to scaled pressure coordinates. The Boussinesq approximation used here would quantitatively alter the relative strength of flow fields between different levels, but do not change the main results qualitatively. Table.1 summarizes all constant and physical scaling of synoptic- and meso-scale variables in the MESD model.

a. Mesoscale disturbances propagating at a tilt angle

In the tropics, MCSs are observed to propagate at various tilt angles to the zonal direction (Houze 1975, 1977, 2004), so it is necessary to investigate the upscale impact on the synoptic-scale circulation of mesoscale disturbances that propagate at various tilt angles. The model setup for mesoscale dynamics follows Yang and Majda (2018), and Figs.2-4 are just altered from Figure 2-4 of Yang and Majda (2018).

In Fig.2a, the red arrow indicates the direction of horizontal propagation of the mesoscale disturbances propagate horizontally. A reference frame with x'- and y'-axis is introduced so that mesoscale disturbances propagate along the positive direction of the x'-axis. The mesoscale heating is prescribed by the first- and second-baroclinic modes in Fig.2b, whose explicit expressions are included in Table.2. The front-to-rear tilted mesoscale heating mimics the life cycle that ranges from congestus to deep to stratiform clouds, and its top-heavy vertical structure is consistent with the observed fact that stratiform precipitation contributes up to 40 percent of the total precipitation in MCSs (Houze 1977). The mesoscale heating is uniform along the direction perpendicular to its propagation direction for simplification purposes.

Fig.3 shows vertical profiles of mesoscale circulation response including zonal and vertical velocity and potential temperature anomalies driven by the mesoscale heating in the x'- and y'-reference frame. As shown by Fig.3a, heating (cooling) regions are dominated by upward and backward (downward and forward) flows throughout the whole troposphere. Low-level inflow is toward heating regions, gradually ascends, and eventually diverges in the upper troposphere. This deep slantwise ascending inflow layer has been shown to be important for maintaining a mature MCS (Moncrieff 1978, 1981; Crook and Moncrieff 1988; Moncrieff 1992). Both zonal and vertical velocities attain maximum strength in the upper troposphere, consistent to the top-heavy vertical profile of mesoscale heating as Fig.2b. As shown by Fig.3b, potential temperature anomalies reach their maximum magnitude in both upper and lower troposphere, significantly dominated by the second baroclinic mode. The vertical profile with warm anomalies on top of cold anomalies resembles realistic features of potential temperature anomalies driven by stratiform precipitation on top of rain evaporation below. Moreover, these anomalies are out of phase with heating/cooling regions with positive anomalies preceding heating regions and trailing cold anomalies (Houze 2004).

b. Upscale impact of mesoscale fluctuations of momentum and temperature

Three eddy terms in the synoptic-scale momentum and thermal equations in Eqs.1a-1c represent upscale impact of mesoscale fluctuations of momentum and temperature that accumulate in time. Yang and Majda (2018) showed that, in general, eddy transfer of horizontal momentum (F^u, F^v)

is along the same direction as the tilt angle γ,

$$\begin{pmatrix} F^u \\ F^v \end{pmatrix} = \kappa^u \left[-\frac{3}{2}\cos(z) + \frac{3}{2}\cos(3z) \right] \begin{pmatrix} \cos(\gamma) \\ \sin(\gamma) \end{pmatrix}, \tag{5}$$

while eddy transfer of temperature is independent of the tilt angle. Here we focus on a tilt angle $\gamma = 0$ (eastward) simply because the remaining tilt angles have the same vertical profiles of eddy transfer of horizontal momentum and just shift their directions by a tilt angle γ. Explicit expressions of eddy transfer of momentum and temperature are included in Table.2.

Fig.4a shows that the vertical profile of eddy transfer of zonal momentum with the tilt angle $\gamma = 0$ attains maximum eastward momentum forcing at height 5 *km*, maximum westward momentum forcing at height 11 *km*, and vanishes at the upper and lower boundaries. The associated eddy momentum fluxes $\overline{u'w'}$ are all negative with maximum strength at the middle troposphere, consistent with the upward (downward) motion being correlated with backward (forward) motion in the heating (cooling) regions as shown in Fig.3. Similar vertical profile of eddy transfer of zonal momentum occur in the idealized two-dimensional cloud resolving simulations of Grabowski and Moncrieff (2001). Fig.4b shows the vertical profile of eddy transfer of temperature with cooling in the middle troposphere and heating in both upper and lower troposphere. In particular, the low-level heating suppresses shallow congestus convection by reducing CAPE and increasing saturation rate of water vapor.

3. Symmetric 2-Day Waves with Embedded Mesoscale Disturbances

In this section, the equations for synoptic-scale dynamics in Eqs.1a-1e model synoptic-scale circulation response to mean heating and upscale impact of embedded mesoscale disturbances that propagate at various directions.

All numerical simulations are conducted in a domain with zonal extent of 15,000 km and vertical extent of 15.7 km. In the meridional direction, the solutions are assumed to decay with latitude. As for numerical resolution, there are a total of 201 x-grids with equally 75 *km* grid spacing and 31 z-grids with equal 0.52 *km* grid spacing. In the meridional direction, the solutions are projected onto the parabolic cylinder functions up to the first 30 modes. The simulations are initialized from the state of rest and ran for 13.83 days to reach a equilibrium state.

a. 2-day waves driven by mean heating

Consistent with the two-scale organization of tropical convection in 2-day waves, the MESD model provides a two-scale framework and simulates 2-day waves as the synoptic-scale circulation response to both mean heating and eddy transfer of momentum and temperature. Here a simple mean heating is prescribed to drive synoptic-scale circulation to capture the leading-order behavior of symmetric 2-day waves observed in nature, including zonal wavelength of 2000-4000 km, westward propagation speed of 10-30 ms^{-1} , tilted middle-heavy heating and equatorial deformation radius of 7° (Takayabu 1994b; Takayabu et al. 1996; Haertel and Kiladis 2004; Kiladis et al. 2009).

Fig.5a shows the vertical profile of prescribed mean heating (measured in time tendency of potential temperature) in the longitude-height diagram, which has zonal wavelength of 3000 *km*, front-to-rear tilts and 18 ms^{-1} westward propagation speed. The mid-heavy heating dominates, accompanied by cooling to the east and west. The meridional profile of mean heating in Fig.5b is assumed to be a Gaussian function e^{-4y^2}, reaching its maximum value at the equator and decaying as the latitude goes poleward.

Fig.6 shows vertical profiles of all flow fields driven by the prescribed mean heating in the longitude-height diagram. As shown in Fig.6a, zonal velocity tilts to the east with height, resembling that observed in nature (Haertel and Kiladis 2004). To the west, surface-level zonal wind convergence occurs near the longitude $X = 7 \times 10^3 km$, with weak zonal wind divergence at its eastern and western sides. As a counterpart, the top-level zonal wind divergence occurs near the longitude $X = 8 \times 10^3 km$. Vertical velocity in Fig.6b has a similar spatial pattern as the mean heating in Fig.5. Dominant upward motion occurs in the middle of the domain with weak downward motion to the east and west. Distinct from the in-phase relation between vertical velocity and mean heating, positive potential temperature anomalies in Fig.6c lead the mean heating to the west, consistent with observations (Haertel and Kiladis 2004). The pressure perturbation in Fig.6d is characterized by negative anomalies at the lower troposphere and positive anomalies in the upper troposphere, both of which have upward and eastward tilts in height. Strong pressure perturbation occurs west of the leading edge of this system.

Fig.7 shows horizontal profiles of horizontal velocity and pressure perturbation at the surface and top of the troposphere. As shown by Fig.7a, convergent winds dominate at the surface with its maximum magnitude at the equator, accompanied by negative pressure perturbation tilting eastward as the latitude goes poleward. The westerly winds at the leading edge to the west is stronger than to the east. Both horizontal winds and pressure perturbation decay poleward. As its counterpart, divergent winds at the top is located to the east of the surface-level wind convergence at the longitude $X = 7.7 \times 10^3 km$. This mean heating driven synoptic-scale circulation response with surface-level (top-level) wind convergence (divergence) resembles the wave train pattern of the 2-day waves observed within a convective envelope (Haertel and Kiladis 2004; Kiladis et al. 2009) *b. Upscale impact of mesoscale disturbances propagating at various tilt angles*

It is critical to understand the upscale impact of mesoscale disturbances that propagate at various tilt angles on symmetric 2-day waves in terms of favorability conditions for convection. Stechmann and Majda (2009) emphasized two factors that could provide favorable conditions for convection, including low-level negative potential temperature anomalies and upward motion. Particularly, three favorable conditions at various levels help interpret the results herein. First, lower-tropospheric (2.62 *km*) negative potential temperature anomaly is favorable for congestus convection through CAPE generation. Secondly, mid-tropospheric inflow (5.24 *km*) increases the entrainment of environmental air and maintains the large CAPE when the environment is moist. Thirdly, upper-tropospheric (7.85 *km*) negative potential temperature anomaly is favorable for deep convection.

Fig.8 shows potential temperature anomalies induced by mean heating and eddy terms at height 2.62 *km* in the longitude-latitude diagram. The potential temperature anomalies in Fig.8a are characterized by alternate anomalies in the zonal direction, particularly with positive (negative) anomalies to the west (east) of wind convergence at $X = 7 \times 10^3 km$, while those induced by eddy terms vary with tilt angle. In the cases where mesoscale disturbances propagate at a tilt angle close to the eastward direction (e.g., 0° and 30°), negative anomalies are induced west of the convective envelope. This provides a favorable condition for congestus convection in a moist environment and promotes the westward propagation of the convective envelope. In contrast, a tilt angle close to the westward direction (e.g., $180^\circ, 150^\circ$) induces positive anomalies in the leading edge, suppressing convection by decreasing CAPE and increasing saturation rate of water vapor. In the intermediate cases (e.g., $60^\circ, 90^\circ, 120^\circ$), positive (negative) anomalies in strong (weak) magnitude are induced in the NH (SH) introduce meridional asymmetry of favorable conditions for convection and explain the southward displacement of observed 2-day waves (Takayabu 1994b; Takayabu et al. 1996; Haertel and Kiladis 2004). Results with the remaining tilt angles (larger than 180°) can be inferred directly from the argument of symmetry.

Cold potential temperature anomalies in the upper troposphere favor deep convection by CAPE buildup. Fig.9 shows horizontal profiles of upper-tropospheric (7.85 *km*) potential temperature anomalies induced by mean heating and eddy terms in the longitude-latitude diagrams. The spatial patterns of potential temperature anomalies induced by eddy terms in Fig.9b-f are similar to those in Fig.8b-f but in the opposite signs, meaning that the associated favorability conditions for convection are simply opposite. In particular, eastward-propagating mesoscale disturbances tend to induce upper-level warm anomalies to the west, suppressing deep convection at the leading edge of the convection envelope.

Fig.10 shows low-level vertical velocity induced by mean heating and eddy terms at height 2.62 *km* at various tilt angles. As shown by Fig.10a, the horizontal profile of vertical velocity resembles that of mean heating with positive anomalies in the middle and negative anomalies on both eastern and western sides. At tilt angles $0° \sim 30°$ in Fig.10b-c, the vertical motion induced by eddy terms is in phase with that induced by mean heating but of opposite sign, weakening vertical motion induced by mean heating. In particular, this extra upward motion at the leading edge mechanically lifts moist air parcels in a moist environment and favors tropical convection as the whole system propagate westward. The effects at tilt angles $120° \sim 180°$ in Fig.10g-h are simply opposite. In the intermediate cases with tilt angles $60° \sim 90°$ in Fig.10d-f, the vertical velocity is significantly reduced by the competing effects between eddy transfer of momentum and temperature.

Fig.11 shows horizontal profiles of surface-level horizontal velocity and pressure perturbation induced by mean heating and eddy terms in the longitude-latitude plane. First, the horizontal velocity induced by eddy terms in Fig.11b-h is much weaker than that induced by mean heating in Fig.11a. Particularly, in the cases with eastward-propagating mesoscale disturbances in Fig.11b, there exists wind convergence to the west and wind divergence to the east, resulting in the westward displacement of total wind convergence relative to the heating center, resembling observations (Haertel and Kiladis 2004). Meanwhile, negative pressure perturbation induced inside the synoptic-scale envelope has a ring shape.

Fig.12 shows horizontal profiles of mid-tropospheric (5.24 *km*) horizontal velocity and pressure perturbation induced by mean heating and eddy terms. Similar to Fig.11a, the horizontal winds induced by mean heating in the middle troposphere in Fig.12a is also characterized by wind convergence in the heating region in weaker magnitude. As for the eddy terms, persistent westerly winds are induced with eastward propagation in Fig.12b. In reality, such extra westerly winds tend to increase the entrainment of environmental air and maintains the large CAPE when the environment is moist. Also, westerly winds in an upward/eastward tilt forms between the surface and the middle troposphere. As for the remaining cases in Fig.12c-h, the resulting wind jets are all along the propagation direction of mesoscale disturbances. Furthermore, a clockwise circulation cell is found at the right side of wind jets. Particularly, in Fig.12d, such cyclonic flows provide favorable conditions for tropical cyclogenesis in the SH.

c. Tilts in the presence of upright mean heating

A key feature of 2-day waves is the front-to-rear tilt throughout the troposphere (Haertel and Kiladis 2004). It is intriguing to investigate whether the tilted vertical structure of synoptic-scale circulation response is induced by mean heating or the upscale impact of mesoscale disturbances. Herein, only cases with upright top-heavy mean heating are considered. This upright mean heating consists of the first- and second- baroclinic modes, $\sin(z) + \alpha\sin(2z)$, $\alpha = -0.5$, representing the significant contribution from deep and stratiform convection in precipitation (Tokay and Short

1996). The results show that even with an upright mean heating, tilted synoptic-scale circulation structure can be realized when the mesoscale disturbances travel in certain directions.

Fig.13 shows vertical profiles of potential temperature anomalies induced by the upright mean heating and eddy terms in the longitude-height diagram. As shown by Fig.13a, the mean heating potential temperature anomalies are characterized by warm (cold) anomalies in the upper (lower) troposphere, resembling upper-tropospheric stratiform heating and lower-tropospheric cooling due to rain evaporation. For the $90^\circ \sim 180^\circ$ tilt angle range in Fig.13c-d, potential temperature anomalies to the west are dominated by the third-baroclinic mode, while those to the east are weak. In the case with the tilt angle 60° in Fig.13e, these anomalies in the third-baroclinic mode is located to the east. Potential temperature anomalies in the case with the tilt angle 0° in Fig.13f have similar spatial pattern to the further east. As for total potential temperature anomalies, the upward/eastward tilted structure with positive anomalies on top of negative anomalies only occurs at tilt angles 60° in Fig.13i and 0° in Fig.13j.

4. Asymmetric 2-day Waves with Embedded Mesoscale Disturbances during Boreal Summer

The effects of the Coriolis force on the synoptic-scale circulation increases with latitude Synoptic-scale circulation, in regard to winds, pressure and potential temperature. The goal of this section is to consider the scenario when both mean heating and mesoscale heating are located to the north of the equator, mimicking 2-day waves that propagate in the NH during boreal summer. It is intriguing how the upscale impact of mesoscale disturbances in asymmetric 2-day waves differs from that in the symmetric waves. Here the mean heating has the same vertical profile as Fig.5a and the asymmetric meridional profile prescribed by a Gaussian function $e^{-4(y-0.5)^2}$, shown in Fig.5b. The 750 *km* (0.5 in dimensionless units) northward displacement of the maximum value is consistent with variance distribution in Kiladis et al. (2009).

Fig.14 shows the horizontal profiles of horizontal winds and pressure perturbation as driven by the mean heating. Besides the convergent winds at the surface, significant cyclonic flows accompanied by negative pressure perturbation are induced at the leading edge of the convective envelope and its northern side under the Coriolis force. Both cyclonic flows and negative pressure perturbations induced by mean heating provide favorable conditions to precondition hurricane embryo, a similar mechanism for tropical cyclogenesis due to wave activity (Frank and Roundy 2006). As a counterpart, divergent winds accompanied by anticyclonic flows and positive pressure perturbation occur at the top of the domain. Besides, the winds to the north of heating center at higher latitudes are stronger than those at lower latitudes in the NH, indicating intensified 2-day waves off the equator.

Fig.15 shows potential temperature anomalies in the lower troposphere in height 2.62 *km* induced by eddy terms at various tilt angles in the longitude-latitude diagram. In the cases with tilt angles ($0^\circ \sim 90^\circ$), the cold potential temperature anomalies induced to the west trigger shallow congestus convection at the leading edge of the convective envelope and promote its westward propagation in a moist environment. Extra warm anomalies are induced at higher latitudes of the NH, suppressing convection off the equator and maintaining its location close to the equator. The cases with $90^\circ \sim 270^\circ$ tilt angles have the opposite effects for equatorial convection by suppressing convection at the leading edge of the convective envelope and triggering shallow congestus convection to the east at the trailing edge. Extra warm anomalies occur at higher NH latitudes, while those at the SH are negligible. In the cases with tilt angles ($270^\circ \sim 0^\circ$), warm anomalies are induced close to the equator, while cold anomalies in weak magnitude are induced at higher latitudes of the NH, which provide favorable conditions for convection off the equator and maintain its northward displacement in asymmetric 2-day waves.

Tropical cyclogenesis

The substantial meridional asymmetry due to the northward displacement of the heating center should occur at all levels of the synoptic-scale circulation response. As shown above, the mean heating driven circulation provides favorable conditions for tropical cyclogenesis with cyclonic flows and negative pressure perturbation. It is important to investigate whether the upscale impact of mesoscale disturbances in the meridionally asymmetric 2-day waves can also influence tropical cyclogenesis by modifying the morphology of synoptic-scale circulation.

Fig.16 shows horizontal profiles of mid-tropospheric horizontal velocity and pressure perturbation induced by mean heating and eddy terms at height 5.24 *km*. The mean heating driven horizontal velocity at the middle troposphere in Fig.16e is characterized by convergent winds in the heating center, accompanied by cyclonic flows and negative pressure perturbation, similar to that at the surface in Fig.14a. As for that induced by eddy terms at various tilt angles in Fig.16a-d and f-h, the resulting horizontal velocity is generally characterized by persistent strong jets along the same propagation direction as mesoscale disturbances. Intuitively, this is consistent with the mid-tropospheric momentum forcing from eddy transfer of horizontal momentum in Fig.4a. Under this extra momentum forcing, those persistent jets actually blow from negative pressure perturbation regions to positive pressure perturbation regions.

More importantly, in the cases with tilt angles ($315^\circ \sim 0^\circ$) in Fig.16f and h, the horizontal jets are accompanied by both cyclonic flows and negative pressure perturbation at their right side in the NH, which preconditions tropical cyclogenesis and explains the prevailing tropical cyclones in the ITCZ regions during boreal summer (Frank and Roundy 2006). These favorable preconditioning conditions for tropical cyclogenesis due to the upscale impact of mesoscale disturbances are distinguished from all other mechanisms such as the vertically sheared horizontal flows (Majda et al.

2008). At the remaining tilt angles, the horizontal jets are accompanied by anti-cyclonic flows and positive pressure perturbation, thus suppressing tropical cyclogenesis.

5. Upscale Impact of Mesoscale Disturbances on 2-Day Waves Versus CCKWs

The MESD model is now used to simulate 2-day waves and CCKWs under the similar model setup (Yang and Majda 2018), except for their opposite propagation speeds (15 ms^{-1} for CCKWs and -18 ms^{-1} for 2-day waves). An intriguing issue concerns differences in the upscale impact of mesoscale disturbances such as convective organization and tropical cyclogenesis. The theoretical predictions about upscale impact of mesoscale disturbances on symmetric westward-propagating 2-day waves and eastward-propagating CCKWs by the MESD model are compared, in terms of the propagation speed of mesoscale disturbances s and propagation direction (tilt angle) γ. A brief summary about asymmetric 2-day waves is also provided.

Table.3 compares the upscale impact of mesoscale disturbances that propagate at various tilt angles and speeds on symmetric 2-day waves and CCKWs in terms of favorability for convection. Both slow propagation ($s < 12m/s$) and fast propagation ($s \geq 12m/s$) scenarios are considered. According to Yang and Majda (2018), the ratio of eddy transfer of temperature and momentum in dimensionless units is proportional to the propagation speed of mesoscale disturbances s. In the slow propagation scenario, eddy transfer of momentum dominates the upscale impact due to mesoscale fluctuations. By comparing Fig.6 in Yang and Majda (2018) and Fig.8 here, their favorability conditions for convection are opposite with a clear east-west contrast. For 2-day waves, low-level negative potential temperature anomalies are induced in the leading edge of the convective envelope only when the mesoscale disturbances propagate at tilt angles ($315^\circ \leq \gamma < 0^\circ$ and $0^\circ \leq \gamma < 45^\circ$), providing favorable conditions for convection. In contrast, for CCKWs, these occurs only when mesoscale disturbances propagate at tilt angles $135^\circ \leq \gamma < 225^\circ$. For both 2-day waves and CCKWs, the northward ($45^\circ \leq \gamma < 135^\circ$) and southward ($225^\circ \leq \gamma < 315^\circ$) propagating mesoscale disturbances tend to suppress convection in one hemisphere and trigger convection in the other, introducing meridional asymmetry. In the fast propagation scenario, eddy transfer of temperature with low-level positive anomalies dominates, providing unfavorable conditions for convection.

Table.4 compares the upscale impact of mesoscale disturbances on symmetric 2-day waves and CCKWs in terms of mid-tropospheric winds and pressure perturbation at height 5.24 km. For 2-day waves, mesoscale disturbances propagating at tilt angles ($315^\circ \leq \gamma < 0^\circ$ and $0^\circ \leq \gamma < 45^\circ$) induce westerlies, strengthening the inflow to 2-day waves from the west to the east. Such strengthening also occurs for CCKWs as mesoscale disturbances propagating at tilt angles ($135^\circ \leq \gamma < 225^\circ$) . In contrast, weakening inflow scenarios occurs at tilt angles ($135^\circ \leq \gamma < 225^\circ$) for 2-day waves and ($315^\circ \leq \gamma < 0^\circ$ and $0^\circ \leq \gamma < 45^\circ$) for CCKWs. For 2-day waves, both north-eastward and south-eastward propagating mesoscale disturbances induce jets accompanied by cyclonic flows, while north-westward and south-westward propagating mesoscale disturbances tend to induce jets accompanied by anti-cyclonic flow. In contrast, for CCKWs, those cyclonic flows do not occur. As far as tropical cyclogenesis is concerned, cyclonic flow is induced in the SH (NH) as mesoscale disturbances propagate at tilt angles $45^\circ \leq \gamma < 90^\circ$ ($270^\circ \leq \gamma < 315^\circ$) in 2-day waves. For CCKWs, negative pressure perturbation is induced at the leading edge of CCKWs as mesoscale disturbances propagate at tilt angles ($135^\circ \leq \gamma < 225^\circ$); that is, favorable conditions for tropical cyclogenesis.

Table.5 describes the upscale impact of mesoscale disturbances that propagate at various tilt angles on asymmetric 2-day waves. As far as favorability conditions for convection is concerned, favorable conditions occur only when mesoscale disturbances propagate at tilt angles ($0^\circ \leq \gamma < 90^\circ$), exhibiting major meridional asymmetry. As a counterpart, the upscale impact of mesoscale disturbances that propagate at tilt angles $270^\circ \leq \gamma < 360^\circ$ suppresses convection near the equator and furthermore trigger shallow congestus convection in the NH at tilt angles $315^\circ \leq \gamma < 360^\circ$. The cases at remaining tilt angles have unfavorable conditions for convection. As for the morphology of circulation, strengthening westerly inflow is induced only when mesoscale disturbances propagate at tilt angles ($0^\circ \leq \gamma < 45^\circ$). The cases with tilt angles ($45^\circ \leq \gamma < 180^\circ$) are characterized by north-eastward/north-westward jets accompanied by anticyclonic flows and positive pressure perturbation in the NH, while those with tilt angles ($180^\circ \leq \gamma < 315^\circ$) have south-westward/south-eastward jets accompanied by positive pressure perturbation. In the cases with tilt angles ($315^\circ \leq \gamma < 360^\circ$), both cyclonic flows and negative pressure perturbation are induced along with east-southward jets in the NH, thereby preconditioning tropical cyclogenesis. Such a scenario with favorable conditions for tropical cyclogenesis due to upscale impact of mesoscale disturbances is distinguished from either symmetric 2-day waves and CCKWs, highlighting unique multi-scale features of asymmetric 2-day waves.

6. Concluding Discussion

As major components of synoptic variability of tropical convection, 2-day waves typically propagate westward in the form of superclusters, containing embedded mesoscale disturbances moving at various tilt angles. It is crucial to understand the multi-scale interactions of tropical convection across the mesoscale and synoptic scale associated with 2-day waves. The goals of this paper include the following four aspects: first, using a simple multi-scale framework to model the synoptic-scale 2-day waves with embedded mesoscale disturbances; Secondly, assessing upscale impact of those mesoscale disturbances that propagate at various tilt angles on 2-day waves in terms of favorability conditions for convection, characteristic morphology of circulation and tropical cyclogenesis; Thirdly, investigating the upscale impact of mesoscale disturbances on asymmetric

2-day waves that propagate off the equator in the NH. Lastly, comparing different theoretical predictions of the upscale impact of mesoscale disturbances on westward-propagating 2-day waves versus eastward-propagating CCKWs.

We addressed major aspects using the MESD model, originally derived by Majda (2007), to simulate 2-day waves as a synoptic-scale circulation response to mean heating and eddy transfer of momentum and temperature. The latter is generated by mesoscale fluctuations of flow fields associated with mesoscale tropical convective disturbances. The mean heating driven synoptic-scale circulation response successfully captures several realistic features of 2-day waves including surface-level (top-level) wind convergence (divergence) in a front-to-rear tilt, while the circulation response to eddy transfer of momentum and temperature induces winds and potential temperature anomalies of comparable magnitude. The successful applications of the MESD model to simulate 2-day waves here and CCKWs in Yang and Majda (2018) further validate its appropriateness for modeling cluster-supercluster interactions across the mesoscale and synoptic scales. Therefore, it is promising to use the MESD model for simulating other convectively coupled equatorial waves, such as easterly waves that are prevalent in the ITCZ regions (Yang et al. 2003; Serra et al. 2008; Toma and Webster 2010a,b).

As inspired by the fact that MCSs are observed to propagate at various directions in the tropics, the upscale impact of mesoscale disturbances propagating at different tilt angles on mean heating driven circulation response is considered. In particular, in the cases with tilt angles ($315^\circ \sim 360^\circ$ and $0^\circ \sim 45^\circ$), low-level negative potential temperature anomalies at height 2.62 km are induced to the west, triggering shallow congestus convection at the leading edge of the westward-propagating envelope in a moist environment. Meanwhile, westerly inflow of comparable magnitude is induced at the lower troposphere at height 5.24 km, feeding additional moisture to the system as the convective envelope propagates westward. All these favorable conditions for convection due to the upscale impact of mesoscale disturbances identify a new mechanism for favouring of westward inertia-gravity waves over eastward inertia-gravity waves. However, the upscale impact also induces mid-tropospheric warm potential temperature anomalies to the west, which would suppress deep convection by increasing the saturation rate of vapor and decreasing CAPE. Such competing effects between triggering shallow convection at lower troposphere and suppressing deep convection at middle troposphere may be the reason why both eastward- and westward-propagating MCSs are observed inside the convective envelope of 2-day waves (Chen et al. 1996). A comparison of upscale impact of mesoscale disturbances on symmetric 2-day waves and CCKWs shows that favorability for convection, morphology of circulation and tropical cyclogenesis at various tilt angles are opposite to each other simply because their convective envelopes propagate in the opposite direction. These consistent results highlight a general feature of upscale impact of mesoscale disturbances; that is, low-level negative potential temperature anomalies and inflow will always be induced in the direction from where the mesoscale disturbances propagate, triggering shallow congestus convection and advancing the synoptic-scale convective envelope.

Concerning the asymmetric 2-day waves propagating along the ITCZ in the NH, the corresponding upscale impact of mesoscale disturbances exhibit distinct behavior at various tilt angles. Besides “favorable” and “unfavorable” regimes for the westward propagation of convective envelope, an extra regime with tilt angles ($270^\circ \sim 360^\circ$) occurs in the NH by suppressing equatorial convection and triggering shallow congestus convection. This provides a mechanism to maintain the northward displacement of 2-day waves off the equator. Furthermore in the NH, in the cases with tilt angles between $315^\circ \sim 360^\circ$, both cyclonic flows and negative pressure perturbation at low troposphere are induced thereby, preconditioning tropical cyclogenesis. This is a new mechanism to explain the prevalent tropical cyclogenesis in the subtropical regions such as the ITCZ region over the northern WP. This is in addition to mechanisms involving the vertically sheared horizontal flows (Majda et al. 2008) and effects of mesoscale vertical shear and moist microscale hot towers on vortex amplification (Majda et al. 2010).

The eddy transfer of momentum is also referred to convective momentum transport (CMT) in tropical meteorology. Its significant role in driving large-scale circulation is confirmed through momentum budget analysis based on objectively analyzed sounding taken during the TOGA COARE intense observing period (Tung and Yanai 2002a,b). Khouider and Han (2013) shows evidence of energy exchange through momentum transport between small-scale circulation due to mesoscale convection and the propagating synoptic-scale wave based on cloud-resolving weather research and forecast (WRF) simulations. Moncrieff et al. (2017) introduced the multi-scale coherent structure parameterization with a single baroclinic mode for CMT and added it into GCMs to represent the missing effects of organized tropical convection. The explicit expressions of eddy transfer of momentum and temperature from the MESD model in Table.2 provide a dynamically based strategy to improve this parameterization. According to the MESD model, eddy transfer of temperature also arises simultaneously along with eddy transfer of momentum in the synoptic-scale equations in Eqs.1a-1e, and it becomes dominant for the fast propagating regime of mesoscale disturbances (Yang and Majda 2018). The importance of eddy transfer of temperature in both observational studies and parameterization of organized tropical convection is currently underestimated and thus requires further investigation.

The MESD model under the current configuration can be elaborated and generalized in various ways. Instead of prescribing the two-scale heating, it should be promising to couple the MESD model with some active heating function for the cloud life cycle such as the multicloud models (Khouider and Majda 2006c,a,b, 2008a,b; Khouider et al. 2010, 2011). Also, the MESD model emphasizes the upscale impact of mesoscale disturbances from the mesoscale to the synoptic scale, but the modulation effects of synoptic-scale circulation on mesoscale heating are neglected. The full consideration of two-way feedback may provide more realistic 2-day waves. Finally, the MESD model could also be used as a framework to diagnostically analyze multi-scale interactions of tropical convection in observational and reanalysis data.

Acknowledgments. This research of A.J.M. is partially supported by the office of Naval Research ONR MURI N00014-12-1-0912 and the Center for Prototype Climate Modeling (CPCM) in New York University Abu Dhabi (NYUAD) Research Institute. Q.Y. is funded as a postdoctoral fellow by CPCM in NYUAD Research Institute.

References

Andrews, D., and M. McIntyre, 1976a: Planetary waves in horizontal and vertical shear: Asymptotic theory for equatorial waves in weak shear. *Journal of the Atmospheric Sciences*, **33 (11)**, 2049–2053.

Andrews, D., and M. McIntyre, 1978a: Generalized eliassen-palm and charney-drazin theorems for waves on axismmetric mean flows in compressible atmospheres. *Journal of the Atmospheric Sciences*, **35 (2)**, 175–185.

Andrews, D., and M. E. McIntyre, 1976b: Planetary waves in horizontal and vertical shear: The generalized eliassen-palm relation and the mean zonal acceleration. *Journal of the Atmospheric Sciences*, **33 (11)**, 2031–2048.

Andrews, D. G., and M. McIntyre, 1978b: An exact theory of nonlinear waves on a lagrangian-mean flow. *Journal of Fluid Mechanics*, **89 (4)**, 609–646.

Andrews, D. G., and M. McIntyre, 1978c: On wave-action and its relatives. *Journal of Fluid Mechanics*, **89 (4)**, 647–664.

Biello, J. A., and A. J. Majda, 2005: A new multiscale model for the Madden-Julian oscillation. *Journal of the atmospheric sciences*, **62 (6)**, 1694–1721.

Biello, J. A., and A. J. Majda, 2006: Modulating synoptic scale convective activity and boundary layer dissipation in the IPESD models of the Madden-Julian oscillation. *Dynamics of atmospheres and oceans*, **42 (1)**, 152–215.

Biello, J. A., and A. J. Majda, 2010: Intraseasonal multi-scale moist dynamics of the tropical atmosphere. *Communications in Mathematical Sciences*, **8 (2)**, 519–540.

Chen, S. S., and R. A. Houze, 1997: Diurnal variation and life-cycle of deep convective systems over the tropical pacific warm pool. *Quarterly Journal of the Royal Meteorological Society*, **123 (538)**, 357–388.

Chen, S. S., R. A. Houze, Jr., and B. E. Mapes, 1996: Multiscale variability of deep convection in relation to large-scale circulation in TOGA COARE. *Journal of the Atmospheric Sciences*, **53 (10)**, 1380–1409.

Clayson, C. A., B. Strahl, and J. Schrage, 2002: 2–3-day convective variability in the tropical western pacific. *Monthly weather review*, **130 (3)**, 529–548.

Crook, N. A., and M. W. Moncrieff, 1988: The effect of large-scale convergence on the generation and maintenance of deep moist convection. *Journal of the atmospheric sciences*, **45 (23)**, 3606–3624.

Dai, A., 2006: Precipitation characteristics in eighteen coupled climate models. *Journal of Climate*, **19 (18)**, 4605–4630.

Dunkerton, T. J., M. Montgomery, and Z. Wang, 2008: Tropical cyclogenesis in a tropical wave critical layer: Easterly waves. *Atmospheric Chemistry and Physics Discussions*, **8 (3)**, 11 149–11 292.

Dunkerton, T. J., M. Montgomery, and Z. Wang, 2009: Tropical cyclogenesis in a tropical wave critical layer. *Atmospheric Chemistry and Physics*, **9 (15)**, 5587–5646.

Frank, W. M., and P. E. Roundy, 2006: The role of tropical waves in tropical cyclogenesis. *Monthly Weather Review*, **134 (9)**, 2397–2417.

Grabowski, W. W., and M. W. Moncrieff, 2001: Large-scale organization of tropical convection in two-dimensional explicit numerical simulations. *Quarterly Journal of the Royal Meteorological Society*, **127 (572)**, 445–468.

Haertel, P. T., and R. H. Johnson, 1998: Two-day disturbances in the equatorial western pacific. *Quarterly Journal of the Royal Meteorological Society*, **124 (546)**, 615–636.

Haertel, P. T., and G. N. Kiladis, 2004: Dynamics of 2-day equatorial waves. *Journal of the Atmospheric Sciences*, **61 (22)**, 2707–2721.

Haertel, P. T., G. N. Kiladis, A. Denno, and T. M. Rickenbach, 2008: Vertical-mode decompositions of 2-day waves and the Madden-Julian oscillation. *Journal of the Atmospheric Sciences*, **65 (3)**, 813–833.

Houze, R. A., Jr., 1975: Squall lines observed in the vicinity of the researcher during phase III of GATE. *Preprints, 16th Radar Meteorology Conf., Houston, TX, American Meteorological Society*, 206–209.

Houze, R. A., Jr., 1977: Structure and dynamics of a tropical squall-line system. *Monthly Weather Review*, **105 (12)**, 1540–1567.

Houze, R. A., Jr., 2004: Mesoscale convective systems. *Reviews of Geophysics*, **42 (4)**.

Khouider, B., J. Biello, and A. J. Majda, 2010: A stochastic multicloud model for tropical convection. *Communications in Mathematical Sciences*, **8 (1)**, 187–216.

Khouider, B., and Y. Han, 2013: Simulation of convectively coupled waves using WRF: a framework for assessing the effects of mesoscales on synoptic scales. *Theoretical and Computational Fluid Dynamics*, **27 (3-4)**, 473–489.

Khouider, B., and A. J. Majda, 2006a: Model multi-cloud parameterizations for convectively coupled waves: Detailed nonlinear wave evolution. *Dynamics of atmospheres and oceans*, **42 (1)**, 59–80.

Khouider, B., and A. J. Majda, 2006b: Multicloud convective parametrizations with crude vertical structure. *Theoretical and Computational Fluid Dynamics*, **20 (5-6)**, 351–375.

Khouider, B., and A. J. Majda, 2006c: A simple multicloud parameterization for convectively coupled tropical waves. part I: Linear analysis. *Journal of the atmospheric sciences*, **63 (4)**, 1308–1323.

Khouider, B., and A. J. Majda, 2008a: Equatorial convectively coupled waves in a simple multicloud model. *Journal of the Atmospheric Sciences*, **65 (11)**, 3376–3397.

Khouider, B., and A. J. Majda, 2008b: Multicloud models for organized tropical convection: Enhanced congestus heating. *Journal of the Atmospheric Sciences*, **65 (3)**, 895–914.

Khouider, B., A. St-Cyr, A. J. Majda, and J. Tribbia, 2011: The MJO and convectively coupled waves in a coarse-resolution gcm with a simple multicloud parameterization. *Journal of the Atmospheric Sciences*, **68 (2)**, 240–264.

Kiladis, G. N., M. C. Wheeler, P. T. Haertel, K. H. Straub, and P. E. Roundy, 2009: Convectively coupled equatorial waves. *Reviews of Geophysics*, **47 (2)**.

Li, G., and S.-P. Xie, 2014: Tropical biases in CMIP5 multimodel ensemble: The excessive equatorial pacific cold tongue and double ITCZ problems. *Journal of Climate*, **27 (4)**, 1765–1780.

Lin, J.-L., 2007: The double-ITCZ problem in IPCC AR4 coupled gcms: Ocean–atmosphere feedback analysis. *Journal of Climate*, **20 (18)**, 4497–4525.

Lindzen, R. S., 1987: On the development of the theory of the qbo. *Bulletin of the American Meteorological Society*, **68 (4)**, 329–337.

Lussier III, L. L., B. Rutherford, M. T. Montgomery, M. A. Boothe, and T. J. Dunkerton, 2015: Examining the roles of the easterly wave critical layer and vorticity accretion during the tropical cyclogenesis of hurricane sandy. *Monthly Weather Review*, **143 (5)**, 1703–1722.

Majda, A. J., 2007: New multiscale models and self-similarity in tropical convection. *Journal of the atmospheric sciences*, **64 (4)**, 1393–1404.

Majda, A. J., and J. A. Biello, 2004: A multiscale model for tropical intraseasonal oscillations. *Proceedings of the National Academy of Sciences of the United States of America*, **101 (14)**, 4736–4741.

Majda, A. J., and R. Klein, 2003: Systematic multiscale models for the tropics. *Journal of the Atmospheric Sciences*, **60 (2)**, 393–408.

Majda, A. J., M. Mohammadian, and Y. Xing, 2008: Vertically sheared horizontal flow with mass sources: a canonical balanced model. *Geophysical and Astrophysical Fluid Dynamics*, **102 (6)**, 543–591.

Majda, A. J., Y. Xing, and M. Mohammadian, 2010: Moist multi-scale models for the hurricane embryo. *Journal of Fluid Mechanics*, **657**, 478–501.

Majda, A. J., and Q. Yang, 2016: A multiscale model for the intraseasonal impact of the diurnal cycle over the maritime continent on the Madden-Julian oscillation. *Journal of the Atmospheric Sciences*, **73 (2)**, 579–604.

Mapes, B., S. Tulich, J. Lin, and P. Zuidema, 2006: The mesoscale convection life cycle: Building block or prototype for large-scale tropical waves? *Dynamics of atmospheres and oceans*, **42 (1)**, 3–29.

Mapes, B. E., and R. A. Houze, Jr, 1993: Cloud clusters and superclusters over the oceanic warm pool. *Monthly Weather Review*, **121 (5)**, 1398–1416.

Matsuno, T., 1966: Quasi-geostrophic motions in the equatorial area. *J. Meteor. Soc. Japan*, **44 (1)**, 25–43.

Moncrieff, M., 1978: The dynamical structure of two-dimensional steady convection in constant vertical shear. *Quarterly Journal of the Royal Meteorological Society*, **104 (441)**, 543–567.

Moncrieff, M., 1981: A theory of organized steady convection and its transport properties. *Royal Meteorological Society, Quarterly Journal*, **107**, 29–50.

Moncrieff, M., 1985: Steady convection in pressure coordinates. *Quarterly Journal of the Royal Meteorological Society*, **111 (469)**, 857–866.

Moncrieff, M. W., 1992: Organized convective systems: Archetypal dynamical models, mass and momentum flux theory, and parametrization. *Quarterly Journal of the Royal Meteorological Society*, **118 (507)**, 819–850.

Moncrieff, M. W., C. Liu, and P. Bogenschutz, 2017: Simulation, modeling, and dynamically based parameterization of organized tropical convection for global climate models. *Journal of the Atmospheric Sciences*, **74 (5)**, 1363–1380.

Nakazawa, T., 1988: Tropical super clusters within intraseasonal variations over the western pacific. *J. Meteor. Soc. Japan*, **66 (6)**, 823–839.

Plumb, R. A., and R. C. Bell, 1982: A model of the quasi-biennial oscillation on an equatorial beta-plane. *Quarterly Journal of the Royal Meteorological Society*, **108 (456)**, 335–352.

Robert, A., 1982: Cloud clusters and large-scale vertical motions in the tropics. *Journal of the Meteorological Society of Japan*, **60 (1)**.

Roundy, P. E., and W. M. Frank, 2004: A climatology of waves in the equatorial region. *Journal of the atmospheric sciences*, **61 (17)**, 2105–2132.

Schrage, J. M., C. A. Clayson, and B. Strahl, 2001: Statistical properties of episodes of enhanced 2–3-day convection in the indian and pacific oceans. *Journal of climate*, **14 (16)**, 3482–3494.

Serra, Y. L., G. N. Kiladis, and M. F. Cronin, 2008: Horizontal and vertical structure of easterly waves in the pacific ITCZ. *Journal of the Atmospheric Sciences*, **65 (4)**, 1266–1284.

Stechmann, S. N., and A. J. Majda, 2009: Gravity waves in shear and implications for organized convection. *Journal of the Atmospheric Sciences*, **66 (9)**, 2579–2599.

Straub, K. H., and G. N. Kiladis, 2002: Observations of a convectively coupled Kelvin wave in the eastern pacific ITCZ. *Journal of the atmospheric sciences*, **59 (1)**, 30–53.

Takahashi, M., and J. R. Holton, 1991: The mean zonal flow response to rossby wave and gravity wave forcing in the equatorial lower stratosphere: Relationship to the qbo. *Journal of the atmospheric sciences*, **48 (18)**, 2078–2088.

Takayabu, Y. N., 1994a: Large-scale cloud disturbances associated with equatorial waves. part i: Spectral feastures of the cloud disturbances. *Journal of the Meteorological Society of Japan. Ser. II*, **72 (3)**, 433–449.

Takayabu, Y. N., 1994b: Large-scale cloud disturbances associated with equatorial waves. part ii: Westward-propagating inertio-gravity waves. *J. Meteor. Soc. Japan*, **72**, 451–465.

Takayabu, Y. N., K. Lau, and C. Sui, 1996: Observation of a quasi-2-day wave during TOGA COARE. *Monthly weather review*, **124 (9)**, 1892–1913.

Tao, W.-K., and M. W. Moncrieff, 2009: Multiscale cloud system modeling. *Reviews of Geophysics*, **47 (4)**.

Tokay, A., and D. A. Short, 1996: Evidence from tropical raindrop spectra of the origin of rain from stratiform versus convective clouds. *Journal of applied meteorology*, **35 (3)**, 355–371.

Toma, V. E., and P. J. Webster, 2010a: Oscillations of the intertropical convergence zone and the genesis of easterly waves. part I: diagnostics and theory. *Climate dynamics*, **34 (4)**, 587–604.

Toma, V. E., and P. J. Webster, 2010b: Oscillations of the intertropical convergence zone and the genesis of easterly waves part II: numerical verification. *Climate dynamics*, **34 (4)**, 605–613.

Tung, W.-W., and M. Yanai, 2002a: Convective momentum transport observed during the TOGA COARE IOP. part I: General features. *Journal of the atmospheric sciences*, **59 (11)**, 1857–1871.

Tung, W.-W., and M. Yanai, 2002b: Convective momentum transport observed during the TOGA COARE IOP. part II: Case studies. *Journal of the atmospheric sciences*, **59 (17)**, 2535–2549.

Wang, Z., M. Montgomery, and T. Dunkerton, 2010: Genesis of pre–hurricane felix (2007). part i: The role of the easterly wave critical layer. *Journal of the Atmospheric Sciences*, **67 (6)**, 1711–1729.

Wheeler, M., and G. N. Kiladis, 1999: Convectively coupled equatorial waves: Analysis of clouds and temperature in the wavenumber–frequency domain. *Journal of the Atmospheric Sciences*, **56 (3)**, 374–399.

Wheeler, M., G. N. Kiladis, and P. J. Webster, 2000: Large-scale dynamical fields associated with convectively coupled equatorial waves. *Journal of the Atmospheric Sciences*, **57 (5)**, 613–640.

Woelfle, M., S. Yu, C. Bretherton, and M. Pritchard, 2018: Sensitivity of coupled tropical pacific model biases to convective parameterization in CESM1. *Journal of Advances in Modeling Earth Systems*.

Yanai, M., and R. H. Johnson, 1993: Impacts of cumulus convection on thermodynamic fields. *The representation of cumulus convection in numerical models*, Springer, 39–62.

Yang, G.-Y., B. Hoskins, and J. Slingo, 2003: Convectively coupled equatorial waves: A new methodology for identifying wave structures in observational data. *Journal of the atmospheric sciences*, **60 (14)**, 1637–1654.

Yang, G.-Y., B. Hoskins, and J. Slingo, 2007a: Convectively coupled equatorial waves. part I: Horizontal and vertical structures. *Journal of the Atmospheric Sciences*, **64 (10)**, 3406–3423.

Yang, G.-Y., B. Hoskins, and J. Slingo, 2007b: Convectively coupled equatorial waves. part II: Propagation characteristics. *Journal of the Atmospheric Sciences*, **64 (10)**, 3424–3437.

Yang, G.-Y., B. Hoskins, and J. Slingo, 2007c: Convectively coupled equatorial waves. part III: Synthesis structures and their forcing and evolution. *Journal of the Atmospheric Sciences*, **64 (10)**, 3438–3451.

Yang, Q., and A. J. Majda, 2014: A multi-scale model for the intraseasonal impact of the diurnal cycle of tropical convection. *Theoretical and Computational Fluid Dynamics*, **28 (6)**, 605–633.

Yang, Q., and A. J. Majda, 2017: Upscale impact of mesoscale disturbances of tropical convection on synoptic-scale equatorial waves in two-dimensional flows. *submitted to Journal of the Atmospheric Sciences*.

Yang, Q., and A. J. Majda, 2018: Upscale impact of mesoscale disturbances of tropical convection on convectively coupled Kelvin waves. *Journal of the Atmospheric Sciences*, **75 (1)**, 85–111.

Yang, Q., A. J. Majda, and B. Khouider, 2017: ITCZ breakdown and its upscale impact on the planetary-scale circulation over the eastern pacific. *Journal of the Atmospheric Sciences*, **74 (12)**, 4023–4045.

Zhang, C., 2005: Madden-Julian oscillation. *Reviews of Geophysics*, **43 (2)**.

LIST OF TABLES

TABLE 1. Constant and physical scaling of synoptic- and meso- scale variables in the MESD model.

	Physical Variables	Symbolic Notation	Value
Constant	buoyancy frequency	N	$10^{-2}s^{-1}$
	height	H	$\frac{16}{\pi} \approx 5km$
	dry kelvin wave speed	c	$50ms^{-1}$
	Rossby parameter	β	$2.23 \times 10^{-11}s^{-1}m^{-1}$
Synoptic scale	horizontal spatial scale	X, Y	$1500km$
	temporal scale	t	$8.3hrs$
	horizontal velocity	U, V	$5ms^{-1}$
	vertical velocity	W	$1.6 \times 10^{-2}ms^{-1}$
	pressure perturbation	P	$250m^2s^{-2}$
	potential temperature anomalies	Θ	$3.3K$
	thermal forcing	S^θ	$10Kday^{-1}$
Mesoscale	horizontal spatial scale	x, y	$150km$
	temporal scale	τ	$50min$
	horizontal velocity	u, v	$5ms^{-1}$
	vertical velocity	w	$1.6 \times 10^{-1}ms^{-1}$
	pressure perturbation	p	$250m^2s^{-2}$
	potential temperature anomalies	θ	$3.3K$
	thermal forcing	s^θ	$100Kday^{-1}$

TABLE 2. Explicit expressions of mesoscale heating, eddy transfer of horizontal momentum and temperature from Yang and Majda (2018).

Physical Variable	Notation	Explicit Expressions
mesoscale heating	s^θ	$s_\theta = c_0\left[\sin(kx' - \omega\tau)\sin(z) + \alpha\sin(kx' - \omega\tau + \phi_0)\sin(2z)\right]$
eddy transfer of horizontal momentum	(F^u, F^v)	$\begin{pmatrix} F^u \\ F^v \end{pmatrix} = \kappa^u\left[-\frac{3}{2}\cos(z) + \frac{3}{2}\cos(3z)\right]\begin{pmatrix} \cos(\gamma) \\ \sin(\gamma) \end{pmatrix}$
magnitude coefficient of (F^u, F^v)	κ^u	$\kappa^u = \frac{c_0^2 \sin(\phi_0)\alpha k^3}{2(\omega^2 - k^2)(4\omega^2 - k^2)}$
eddy transfer of temperature	F^θ	$F^\theta = \kappa^\theta\left[\frac{3}{2}\sin(z) - \frac{9}{2}\sin(3z)\right]$
magnitude coefficient of F^θ	κ^θ	$\kappa^\theta = \frac{c_0^2 \sin(\phi_0)\alpha k^3 c}{2(\omega^2 - k^2)(4\omega^2 - k^2)}$

TABLE 3. Comparison of upscale impact of mesoscale disturbances on symmetric 2-day waves and CCKWs in terms of favorability for convection. "Favorable" means that the upscale impact induces low-level (2.62 km) negative potential temperature anomalies in the leading edge, providing favorable conditions for convection and promoting forward propagation of synoptic-scale convective envelope, while "unfavorable" has the opposite meaning. Here symmetric 2-day waves refer to westward-propagating 2-day waves with their maximum convection at the equator.

Propagating Speed of Mesoscale Disturbances	Tilt Angle γ	Symmetric 2-Day Wave	CCKW
slow ($s < 12m/s$)	$315^\circ \leqslant \gamma < 360^\circ$, $0^\circ \leqslant \gamma < 45^\circ$	**favorable**	unfavorable
	$45^\circ \leqslant \gamma < 135^\circ$	suppressing (triggering) convection to the north (south)	suppressing convection to the north
	$135^\circ \leqslant \gamma < 225^\circ$	unfavorable	**favorable**
	$225^\circ \leqslant \gamma < 315^\circ$	suppressing (triggering) convection to the south (north)	suppressing convection to the south
fast ($s \geqslant 12m/s$)	all	unfavorable	unfavorable

TABLE 4. Comparison of upscale impact of mesoscale disturbances on symmetric 2-day waves and CCKWs in terms of low-level winds and pressure perturbation at height 5.24 km. The propagation speed of mesoscale disturbances are fixed at 5 m/s. Cyclonic flows and negative pressure perturbation are regarded as favorable conditions to precondition tropical cyclogenesis.

Tilt Angle γ	Symmetric 2-Day Wave	CCKW
$315^\circ \leqslant \gamma < 360^\circ, 0^\circ \leqslant \gamma < 45^\circ$	**strengthening westerly inflow**	weakening easterly inflow
$45^\circ \leqslant \gamma < 90^\circ$	inducing north-eastward jets accompanied by cyclonic flow to the right	inducing westerly winds to the north
$90^\circ \leqslant \gamma < 135^\circ$	inducing north-westward jets accompanied by anti-cyclonic flow to the right	inducing north-westward jets accompanied by anti-cyclonic flows on both sides
$135^\circ \leqslant \gamma < 225^\circ$	weakening westerly inflow	**strengthening easterly inflow**
$225^\circ \leqslant \gamma < 270^\circ$	inducing south-westward jets accompanied by anti-cyclonic flow to the left	inducing south-westward jets accompanied by anti-cyclonic flows on both sides
$270^\circ \leqslant \gamma < 315^\circ$	inducing south-eastward jets accompanied by cyclonic flow to the left	inducing westerly winds to the south
tropical cyclogenesis	by cyclonic flow: $45^\circ \leqslant \gamma < 90^\circ$ in the SH and $270^\circ \leqslant \gamma < 315^\circ$ in the NH	by negative pressure: $135^\circ \leqslant \gamma < 225^\circ$ in the leading edge

TABLE 5. Upscale impact of mesoscale disturbances on asymmetric 2-day waves in terms of favorablility for convection, morphology of circulation and tropical cyclogenesis. "Favorable preconditioning" corresponds to the scenario with cyclonic flows and negative pressure perturbation in the NH that precondition tropical cyclogenesis, while "suppressing" has the opposite meaning. "Neutral" corresponds to the scenario with neither preconditioning nor suppressing conditions for tropical cyclogenesis. Here asymmetric 2-day waves refer to westward-propagating 2-day waves with their maximum convection in the NH.

Asymmetric 2-Day Wave			
Tilt Angle γ	Favorability for Convection	Morphology of Circulation	Tropical Cyclogenesis
$0^\circ \leqslant \gamma < 45^\circ$	**favorable**	**strengthening westerly inflow** and inducing clockwise flows and positive pressure perturbation at the equator	neutral
$45^\circ \leqslant \gamma < 90^\circ$	**favorable**	inducing north-eastward jets accompanied by anti-cyclonic flows and positive pressure perturbation in the NH	suppressing
$90^\circ \leqslant \gamma < 180^\circ$	unfavorable	inducing north-westward jets accompanied by anti-cyclonic flow and positive pressure perturbation in the NH	suppressing
$180^\circ \leqslant \gamma < 270^\circ$	unfavorable	inducing south-westward jets accompanied by positive pressure perturbation at the equator	neutral
$270^\circ \leqslant \gamma < 315^\circ$	suppressing equatorial convection	inducing south-eastward jets accompanied by positive pressure perturbation at the equator	neutral
$315^\circ \leqslant \gamma < 360^\circ$	suppressing equatorial convection, preconditioning shallow congestus convection in the NH	inducing east-southward jets with cyclonic flows and negative pressure perturbation in the NH	**favorable preconditioning**

LIST OF FIGURES

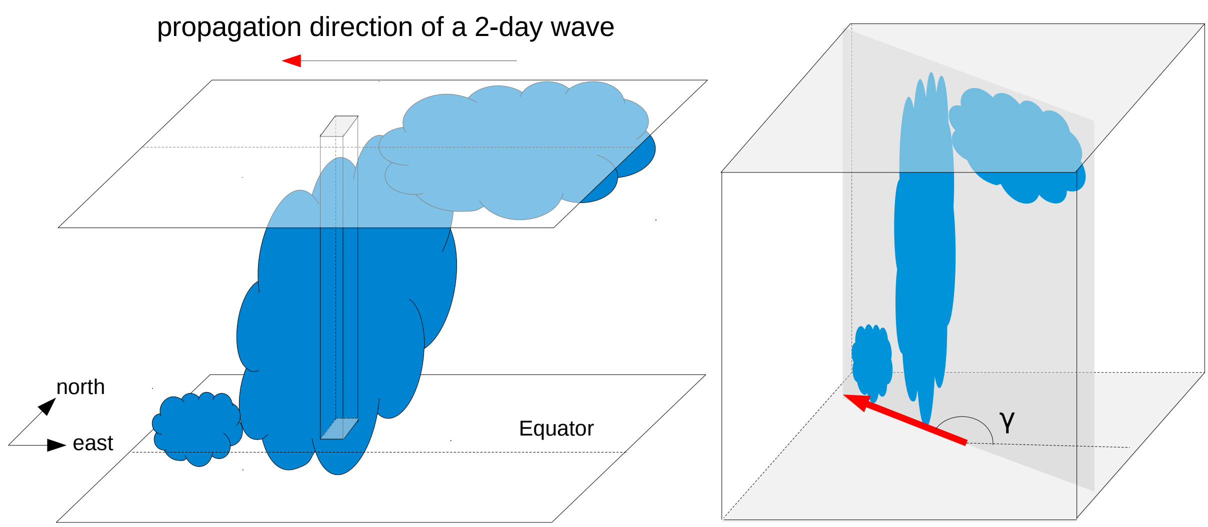

FIG. 1. Conceptual diagram for a 2-day wave with embedded mesoscale disturbances. (left) An westward-moving 2-day wave (blue) on the synoptic scale, where the rectangular cuboid denotes a mesoscale domain. (right) An MCS propagating at a tilt angle γ in the mesoscale domain (zoom in the rectangular cuboid in the left panel).

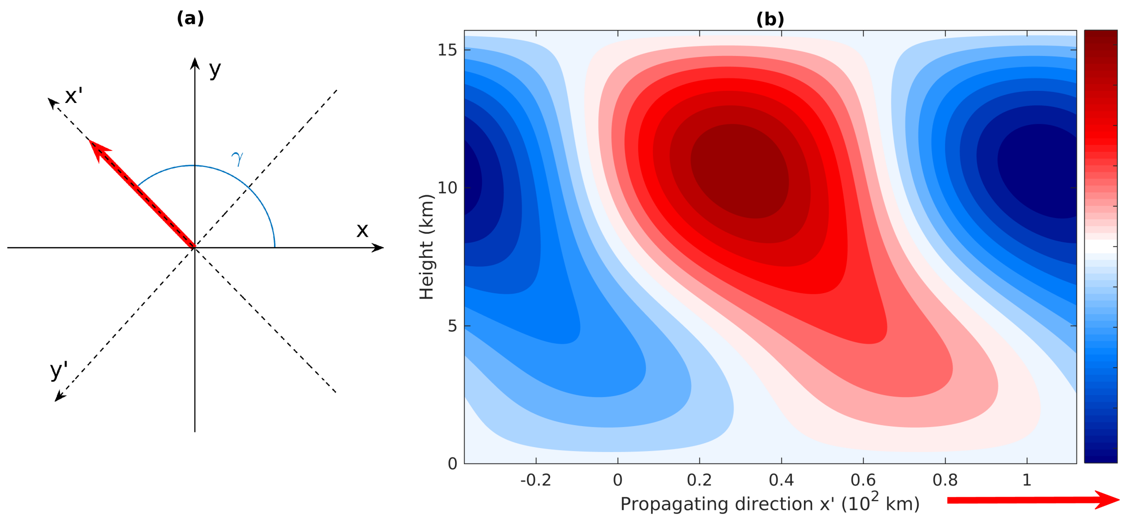

FIG. 2. Vertical profile of mesoscale heating in the new reference frame. In panel (a), the normal reference frame is denoted by x-axis (east) and y-axis (north) in solid lines. The new reference frame with x'-axis and y'-axis in dashed lines is derived by anti-clockwise rotating the normal reference frame by an angle γ. The red bold arrow shows the propagation direction of mesoscale heating. Panel (b) shows the vertical profile of mesoscale heating in the new reference frame. The dimensional unit is 100 $Kday^{-1}$. [from Yang and Majda (2018)]

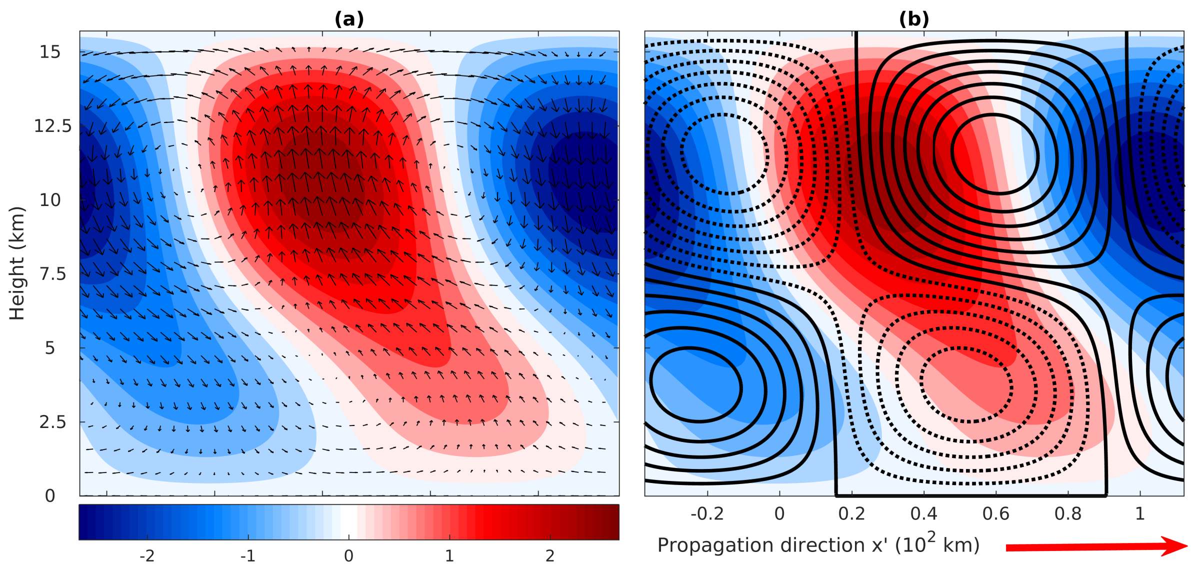

FIG. 3. Vertical profiles of zonal velocity, vertical velocity and potential temperature anomalies along the propagation direction of mesoscale heating. The arrows in panel (a) show zonal and vertical velocity and the contours in panel (b) show potential temperature anomalies. The color in both panels shows mesoscale heating. The maximum magnitudes of zonal and vertical velocity are 3.72 ms^{-1} and 0.47 ms^{-1}, respectively. The contour interval of potential temperature anomalies is 0.1 K. The dimensional unit of mesoscale heating is 100 $Kday^{-1}$. [from Yang and Majda (2018)]

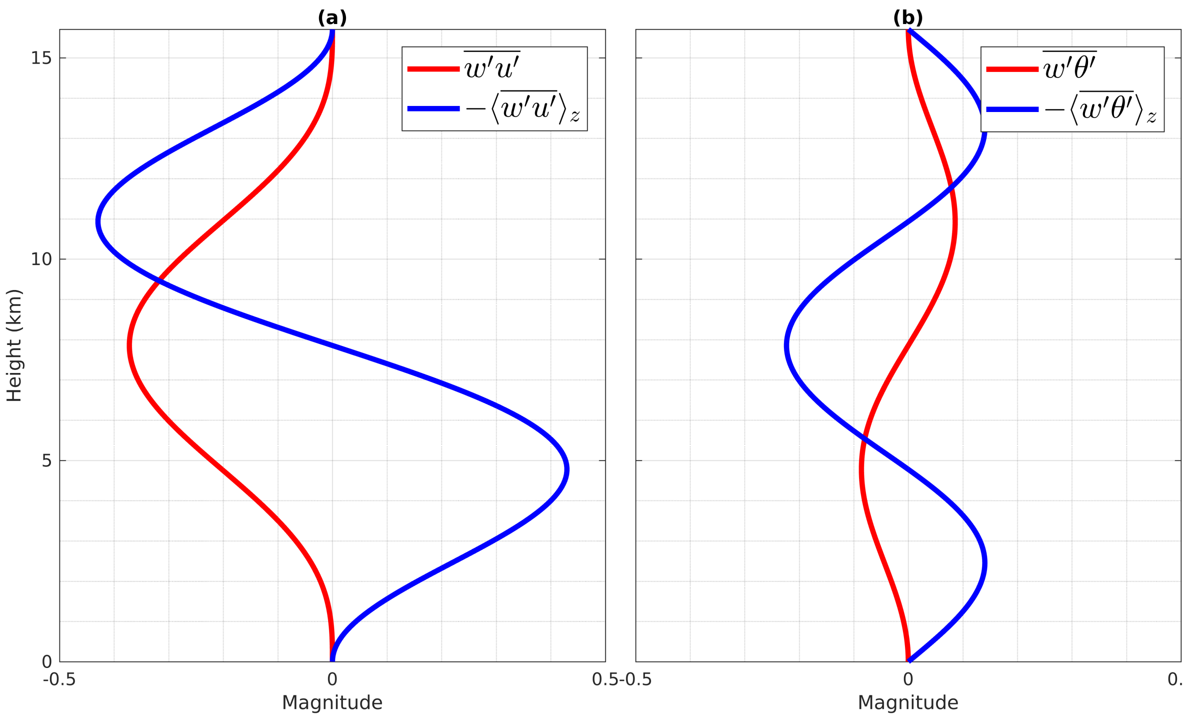

FIG. 4. Vertical profiles of eddy transfer of momentum and temperature in the case with eastward-propagating mesoscale disturbances. Panel (a) shows eddy transfer of zonal momentum (blue) and the associated eddy momentum flux (red). Panel (b) shows eddy transfer of temperature (blue) and the associated eddy heat flux (red). One dimensionless unit of eddy transfer of momentum and temperature is 15 $ms^{-1}day^{-1}$ and 10 $Kday^{-1}$, respectively. [from Yang and Majda (2018)]

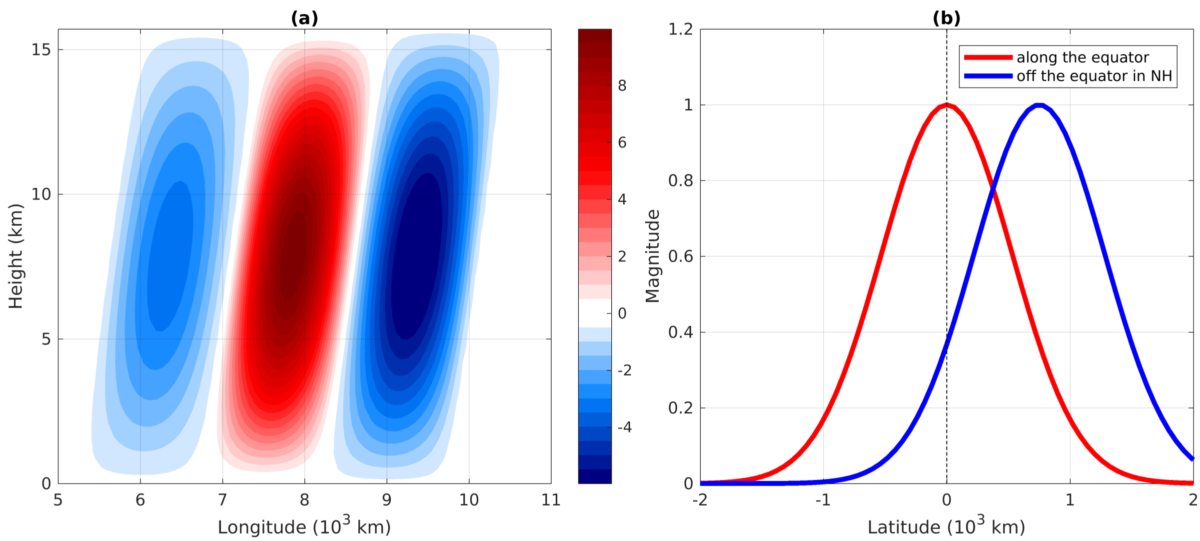

FIG. 5. Spatial structure of prescribed mean heating profile on the synoptic scale. Panel (a) shows its vertical profile along the equator and panel (b) shows its meridional profile in both symmetric and asymmetric cases. The mean heating in panel (a) has dimensional units of $Kday^{-1}$, while that in panel (b) is dimensionless.

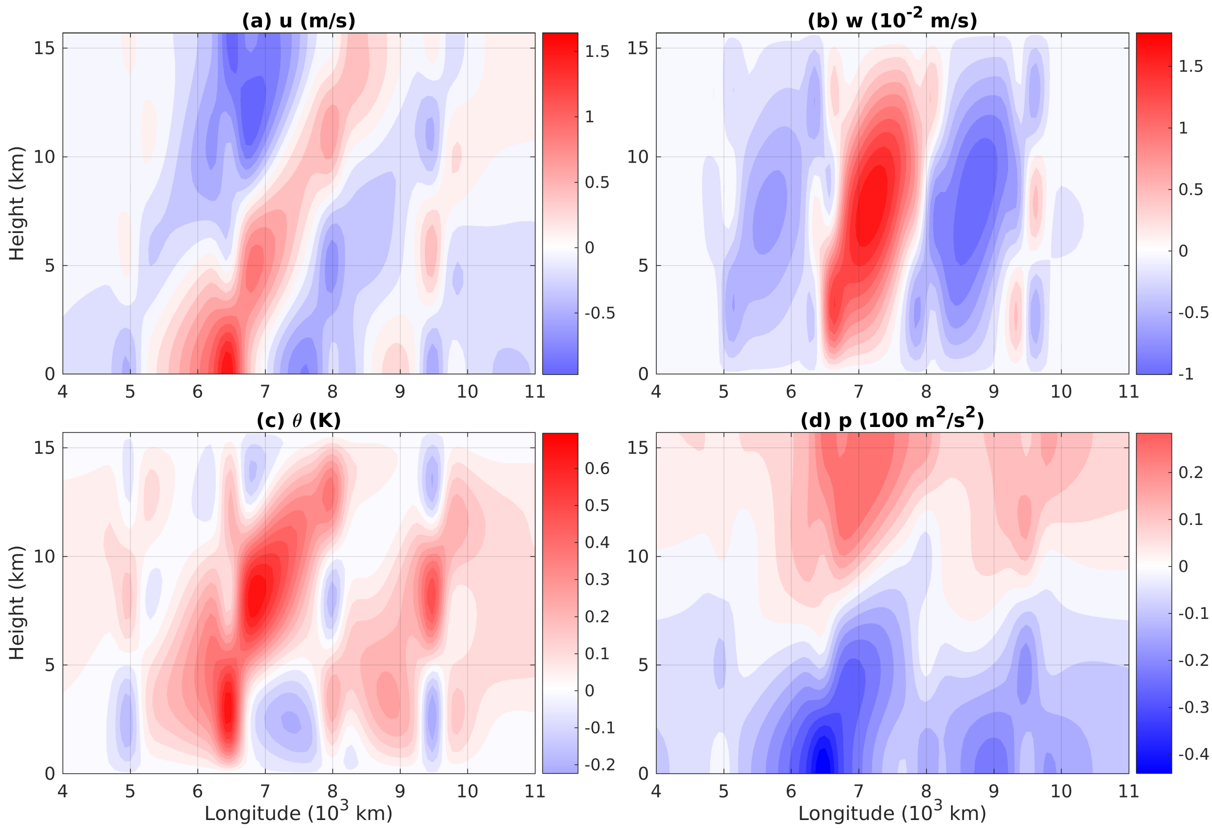

FIG. 6. Vertical cross-sections of mean heating driven flow fields at the equator in the longitude-height diagram. These panels correspond to (a) zonal velocity, (b) vertical velocity, (c) potential temperature anomalies and (d) pressure perturbation. The corresponding dimensional units of these flow fields are indicated in the subtitle of each panel.

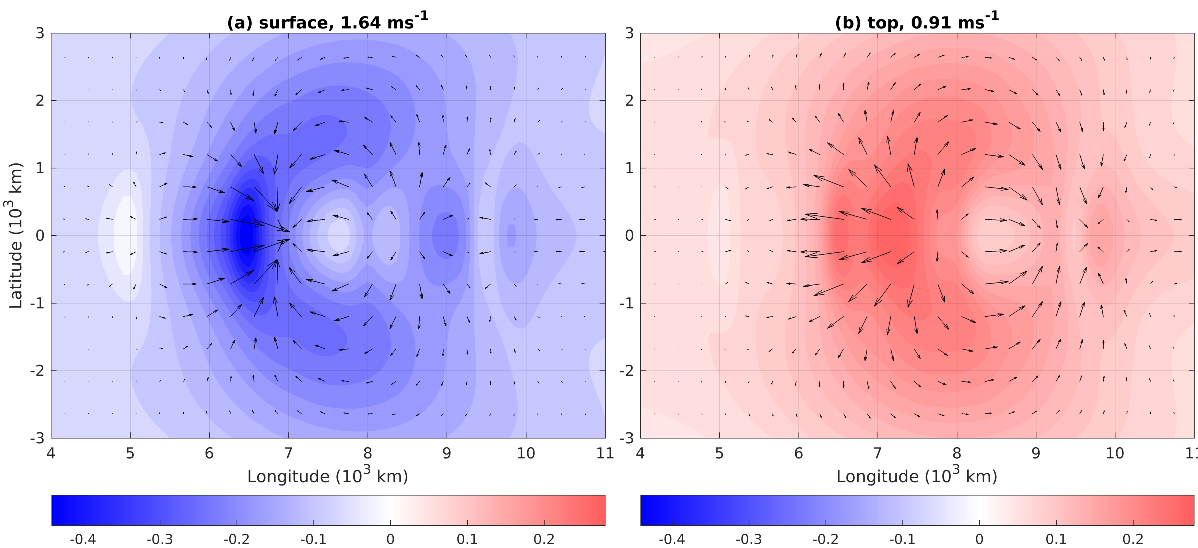

FIG. 7. Horizontal sections of mean heating driven horizontal velocity and pressure perturbation. Panel (a) corresponds to the surface and panel (b) is for the top of the domain. Horizontal velocity is indicated by arrows, while pressure perturbation is indicated by color. The dimensional units of horizontal velocity and pressure perturbation are ms^{-1} and m^2s^{-2}, respectively.

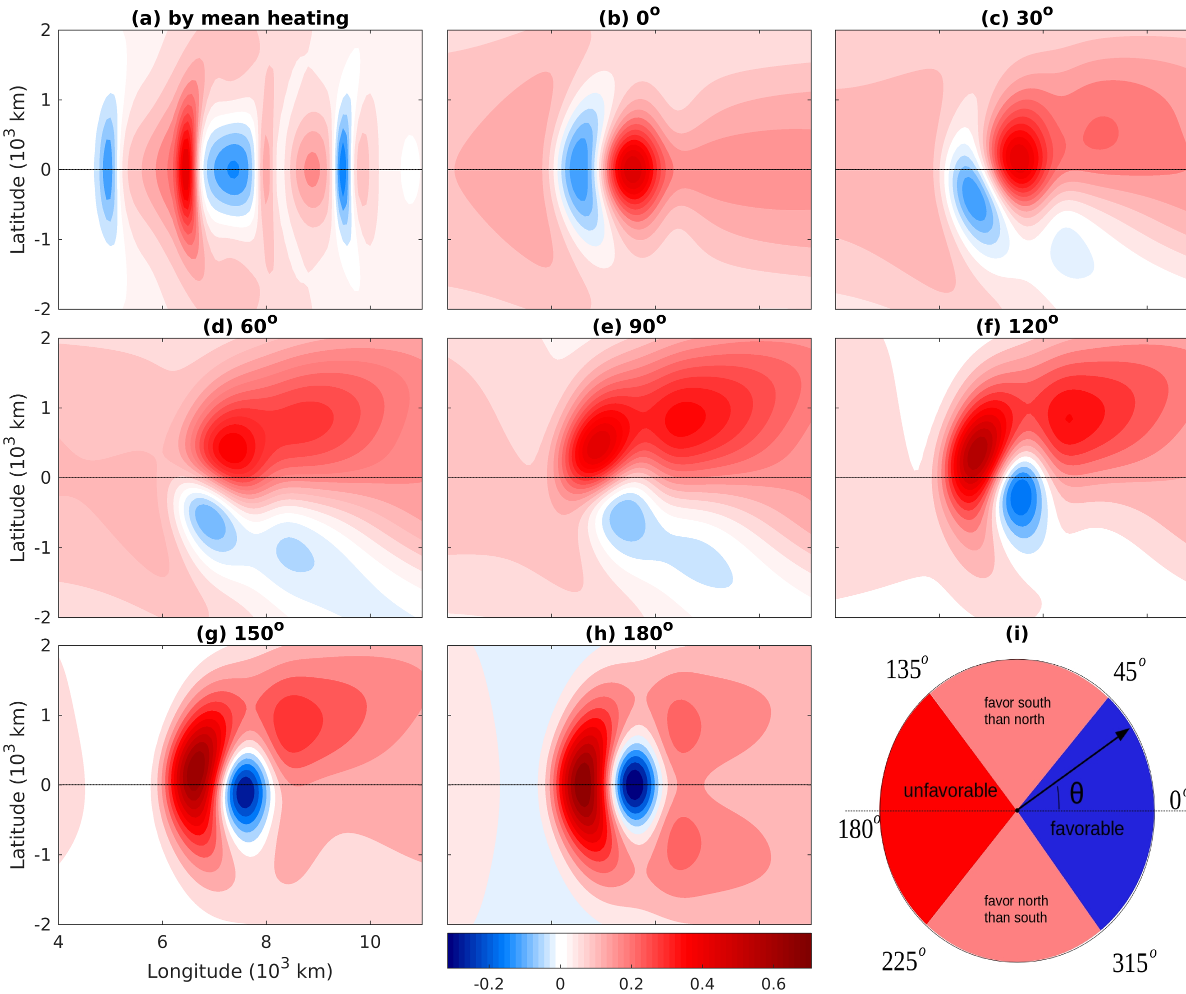

921 FIG. 8. Horizontal sections of potential temperature anomalies in the lower troposphere (2.62 km) in the longitude-latitude diagram. Panel (a) shows anomalies induced by mean heating, while panels (b-h) show anomalies induced by eddy terms at tilt angles from 0° to 180°, respectively. Panel (i) summarizes favorability of convection in different tilt angle cases (blue: favorable; pink: unfavorable, asymmetric; red: unfavorable). The dimensional unit of potential temperature anomalies is K.

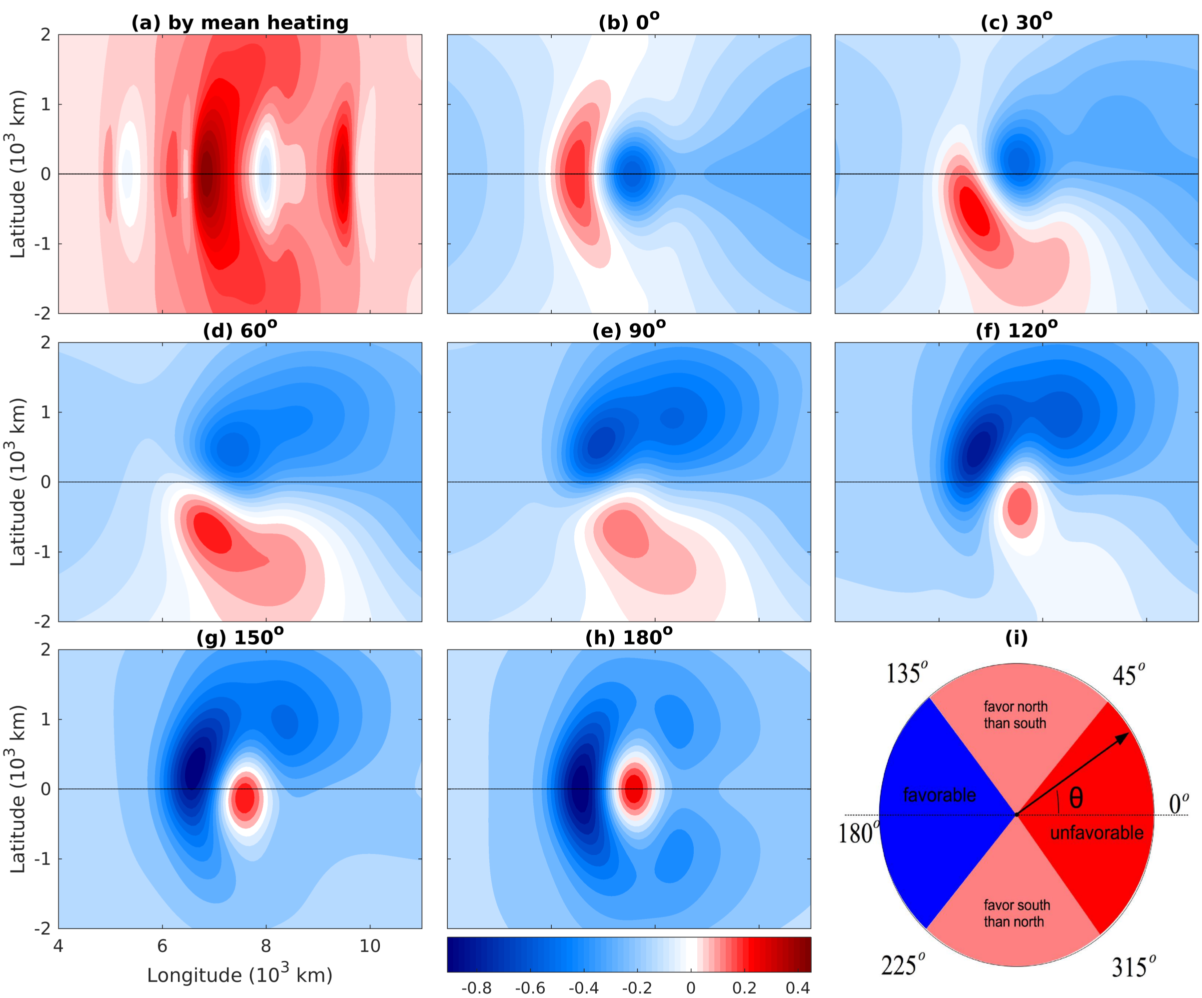

FIG. 9. Similar to Fig.8 but in the upper troposphere (7.85 *km*).

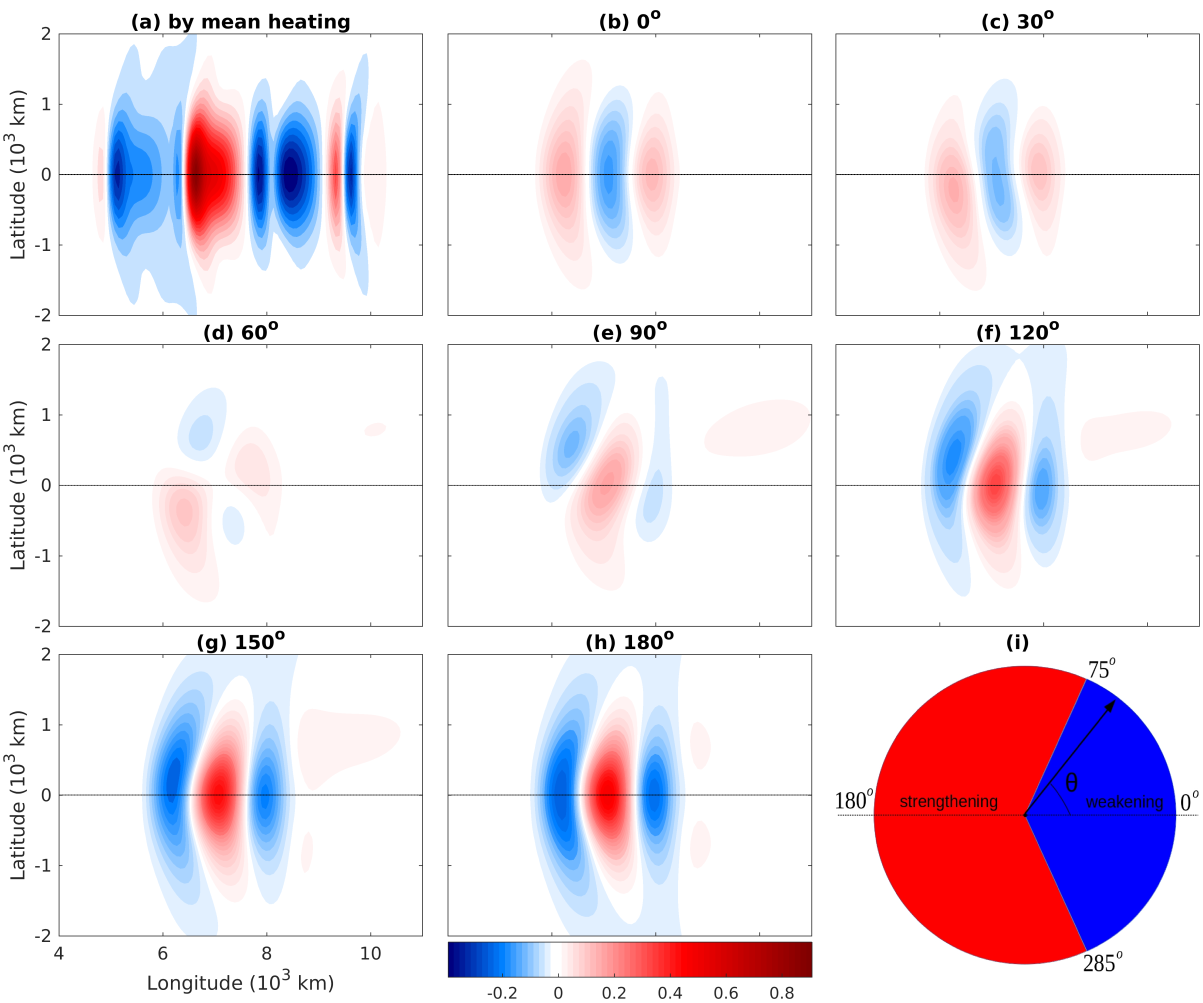

FIG. 10. Similar to Fig.8 but for vertical velocity in the lower troposphere (2.62 *km*). Panel (i) summarizes the impact of eddy driven vertical velocity on mean heating driven vertical velocity (blue: weakening; red: strengthening).

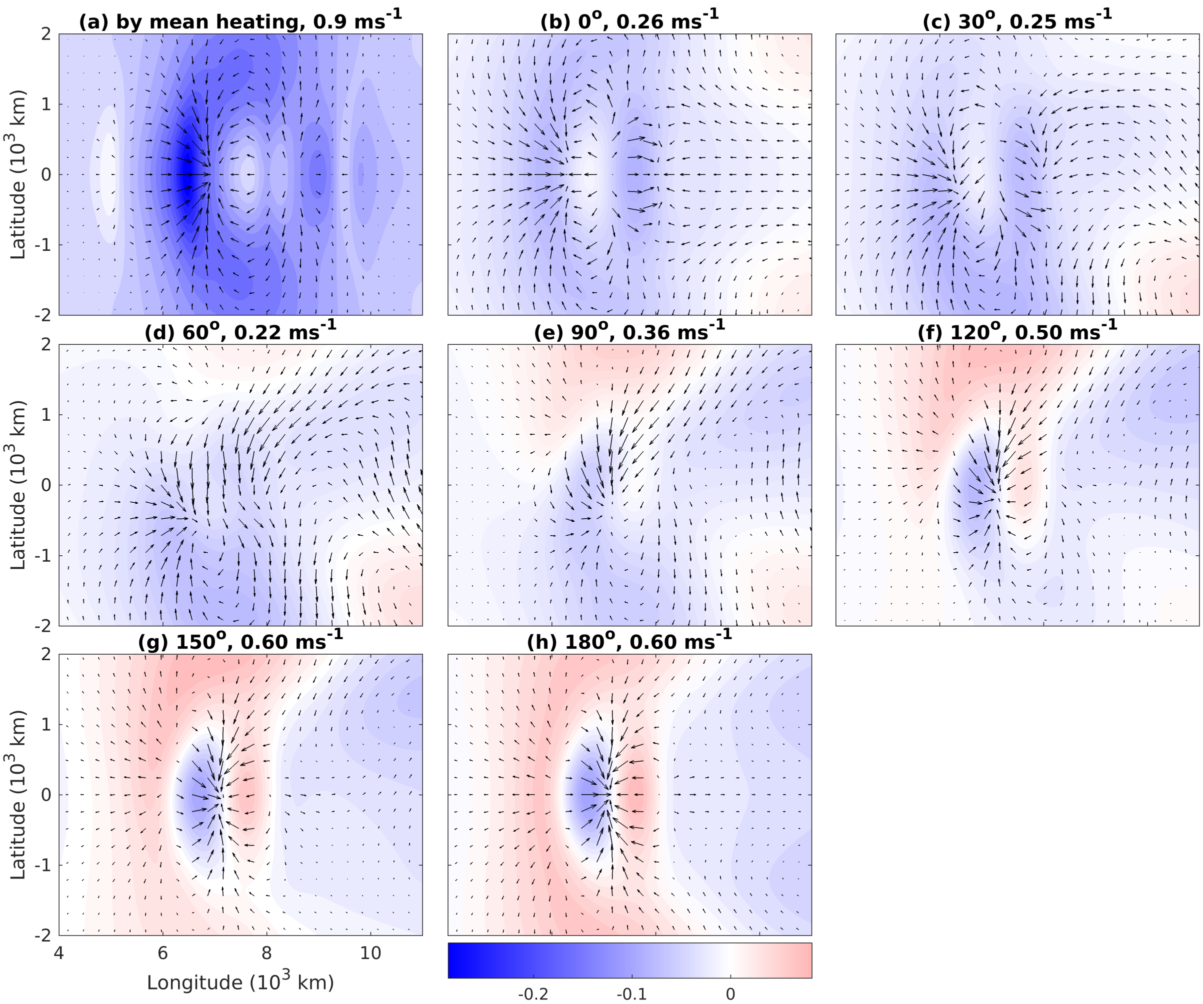

FIG. 11. Horizontal profiles of horizontal velocity and pressure perturbation at the surface (0 *km*) in the longitude-latitude diagrams. Panel (a) shows those induced by mean heating, while panels (b-h) show those induced by eddy terms at tilt angles from 0° to 180°, respectively. Horizontal velocity is shown by arrows and pressure perturbation is shown by color. The maximum magnitude of horizontal velocity is indicated in the subtitle of each panel. The dimensional units of horizontal velocity and pressure perturbation are ms^{-1} and 100 m^2s^{-2}.

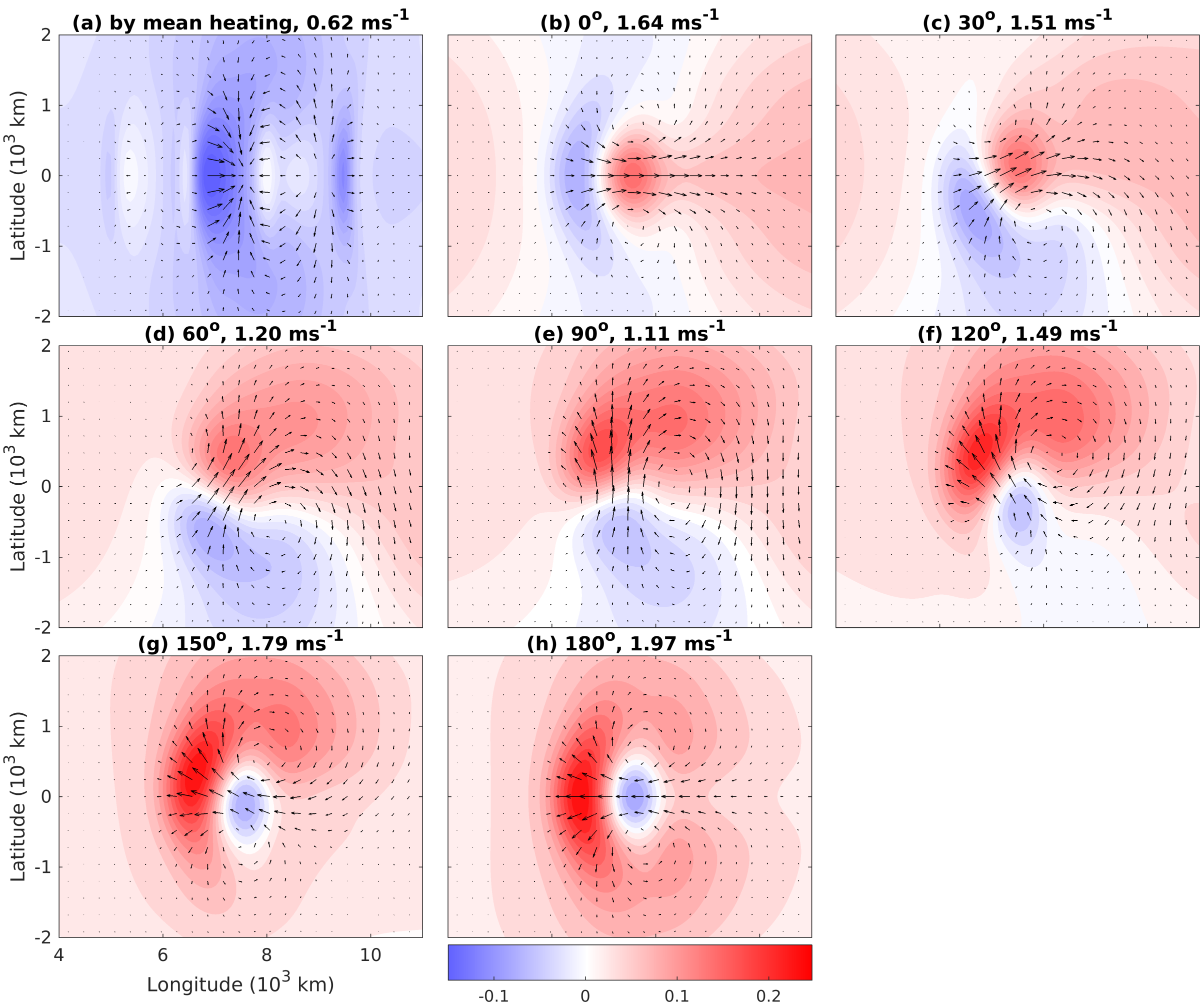

FIG. 12. Similar to Fig.11 but in the middle troposphere (5.24 km).

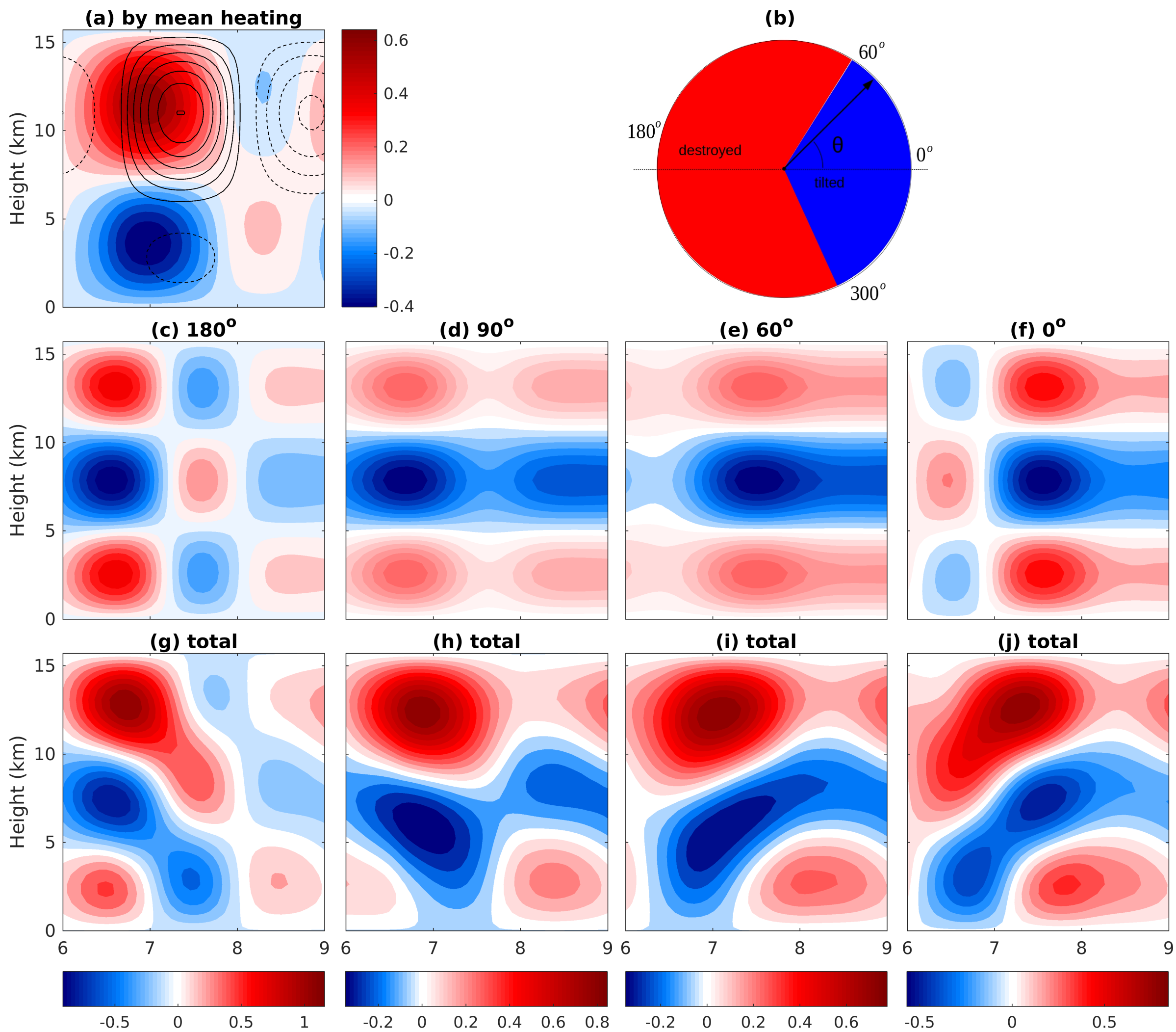

FIG. 13. Vertical profiles of potential temperature anomalies at the equator in the longitude-height diagram. In panel (a), top-heavy upright mean heating is indicated by contours and the resulting anomalies are shown by color. Panels (c-f) show anomalies induced by eddy terms at tilt angles of 180°, 90°, 60° and 0°, respectively. Panels (g-j) show total anomalies induced by both top-heavy upright mean heating and eddy terms in the same column. Panel (b) summarizes the upscale impact of mesoscale disturbances on the vertical structure of potential temperature anomalies (blue: tilted; red: destroyed). The dimensional unit is K.

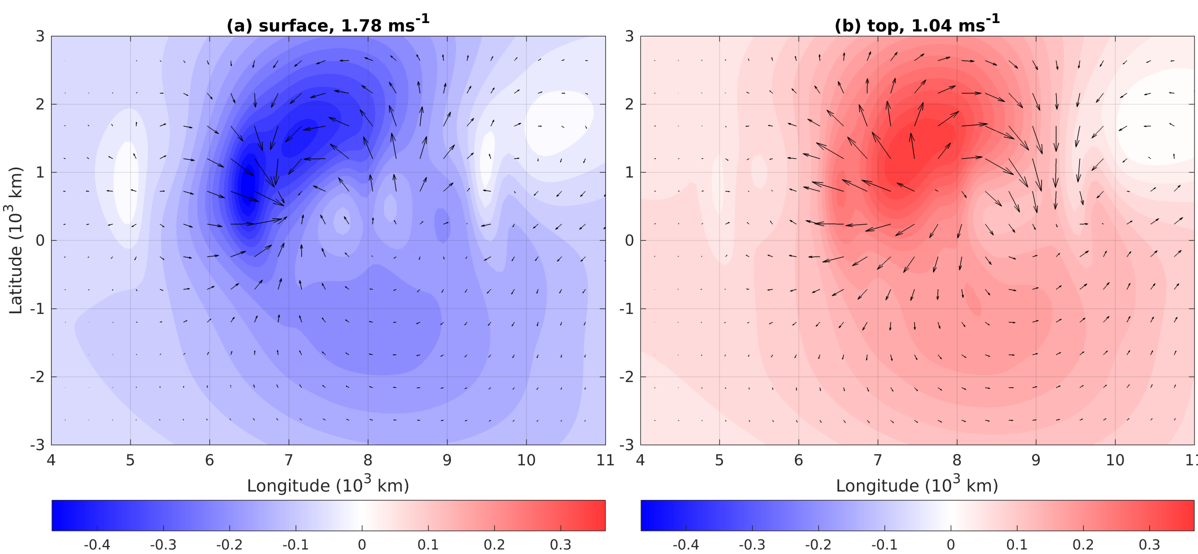

FIG. 14. Similar to Fig.7 but driven by meridionally asymmetric mean heating.

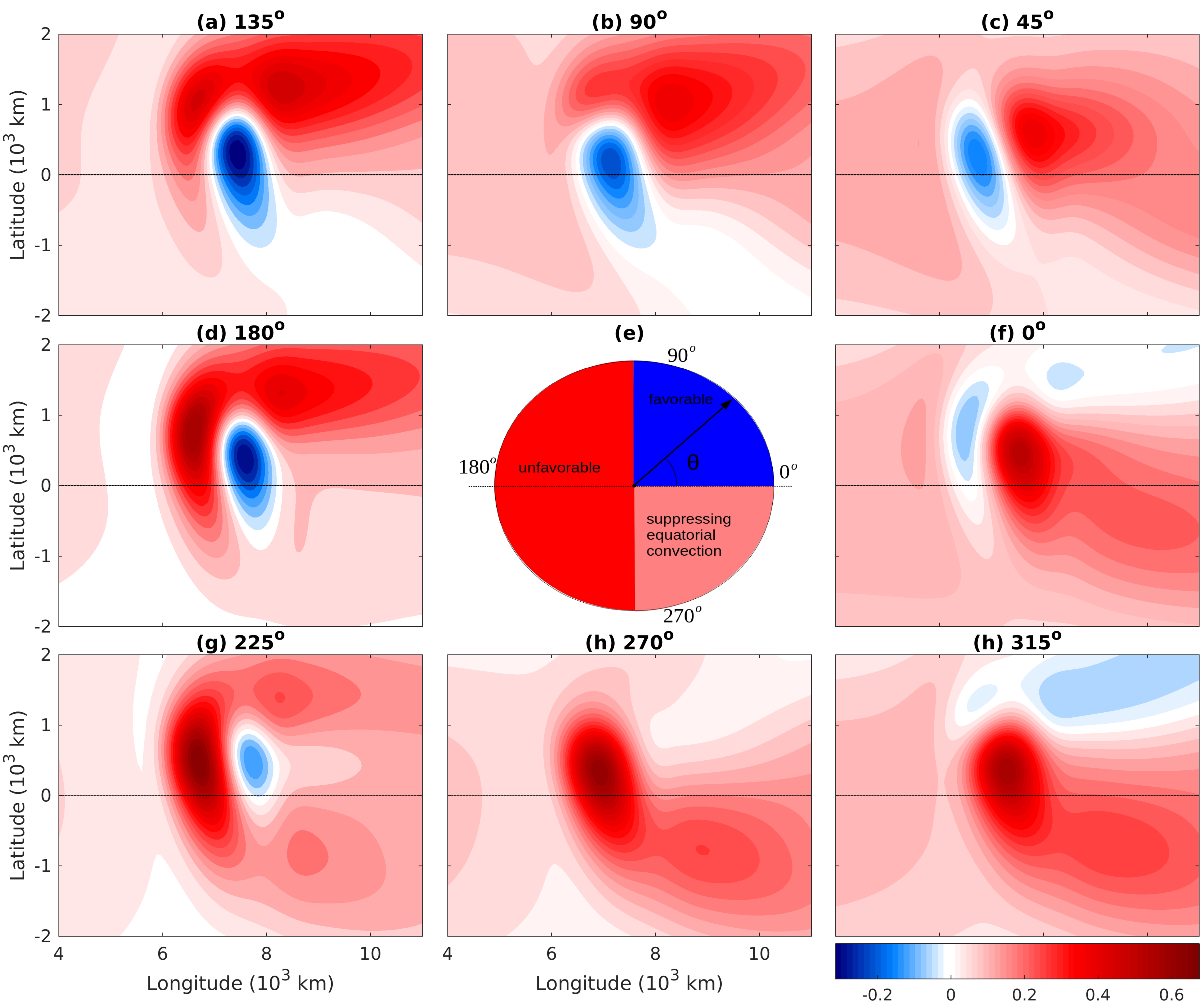

FIG. 15. Similar to Fig.8 but driven by eddy terms modulated by a meridional asymmetric envelope. Panel (e) summarizes favorability of convection in different tilt angle cases (blue: favorable; pink: suppressing equatorial convection; red: unfavorable).

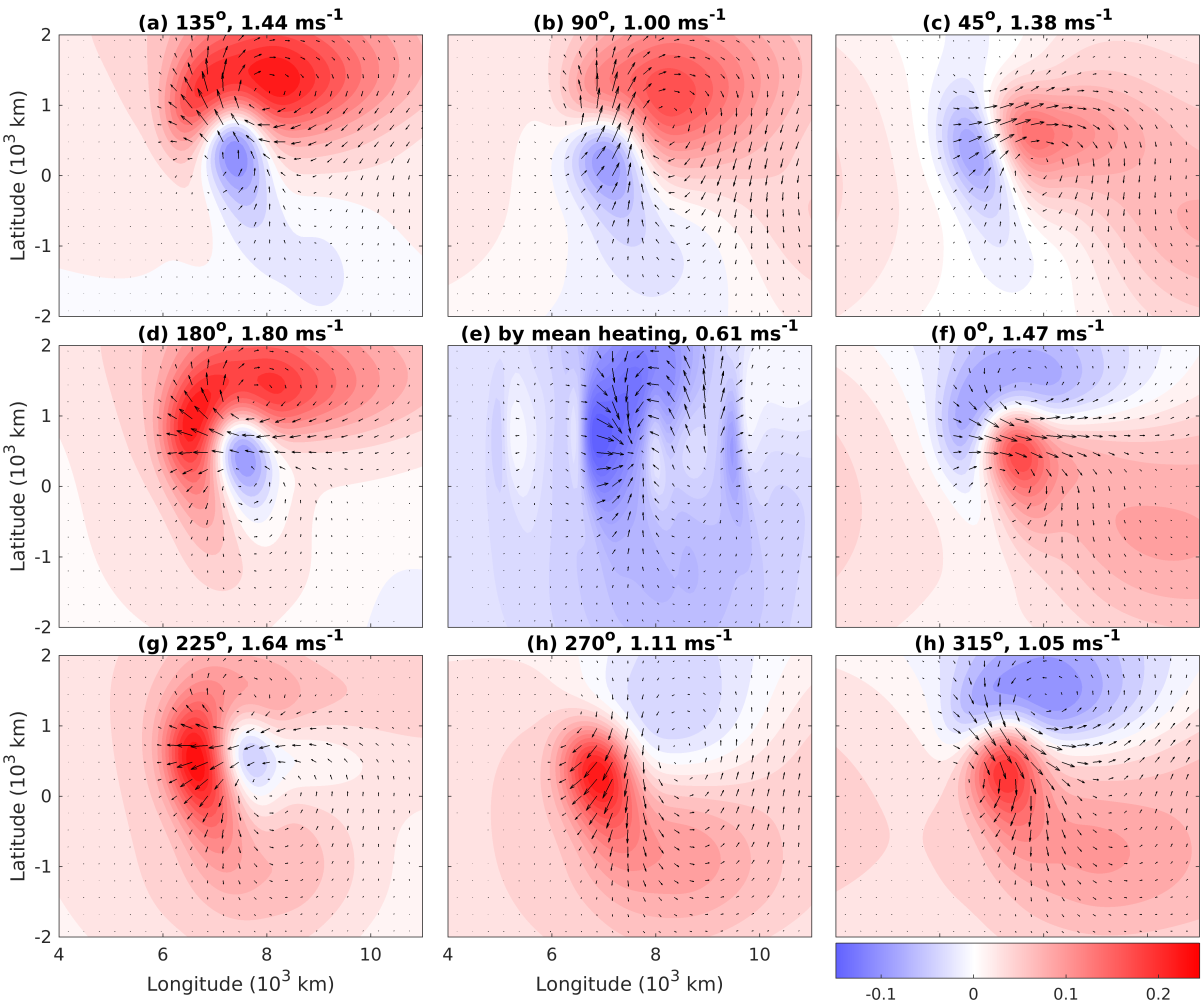

FIG. 16. Similar to Fig.11 but in the middle troposphere (5.24 km) in the meridionally asymmetric case.